Control of Structures and Emission Properties of (CuI) n 2-Methyldithiane Coordination Polymers

Adrien Schlachter, Lydie Viau, Daniel Fortin, Lena Knauer, Carsten Strohmann, Michael Knorr, Pierre Harvey

▶ **To cite this version:**

Adrien Schlachter, Lydie Viau, Daniel Fortin, Lena Knauer, Carsten Strohmann, et al.. Control of Structures and Emission Properties of (CuI) n 2-Methyldithiane Coordination Polymers. Inorganic Chemistry, 2018, 57 (21), pp.13564 - 13576. 10.1021/acs.inorgchem.8b02168 . hal-01935183

HAL Id: hal-01935183
https://hal.science/hal-01935183v1

Submitted on 14 Jan 2022

HAL is a multi-disciplinary open access archive for the deposit and dissemination of scientific research documents, whether they are published or not. The documents may come from teaching and research institutions in France or abroad, or from public or private research centers.

L'archive ouverte pluridisciplinaire **HAL**, est destinée au dépôt et à la diffusion de documents scientifiques de niveau recherche, publiés ou non, émanant des établissements d'enseignement et de recherche français ou étrangers, des laboratoires publics ou privés.

Control of Structures and Emission Properties of $(CuI)_n$ 2-Methyldithiane Coordination Polymers

Adrien Schlachter,[a] Lydie Viau,[b] Daniel Fortin,[a] Lena Knauer,[c] Carsten Strohmann,[c] Michael Knorr,[b]* and Pierre D. Harvey[a]**

[a] Département de Chimie, Université de Sherbrooke, Sherbrooke, Québec, Canada J1K 2R1.

[b] Institut UTINAM UMR CNRS 6213, Université Bourgogne Franche-Comté, 25030 Besançon, France.

[c] Anorganische Chemie, Technische Universität Dortmund, Otto-Hahn-Strasse 6, 44227 Dortmund, Germany

ABSTRACT A structurally unique and strongly luminescent non-porous 3D coordination polymer (CP) $[Cu_8I_8(methyldithiane)_4]_n$**, CP3**, has been prepared in a quasi-anticipated manner from 2-methyl-1,3-dithiane, **L1**, and CuI. This CP incorporates the unprecedented Cu_8I_8 cluster built upon two side-fused open cubanes. The crystal structure of **CP3** has been determined at 100, 150, 200, 250, 300, 350 and 400 K to study the temperature dependence of the Cu···Cu distances. Two other topological 1D and 2D CPs isomers of formula $[\{Cu_2I_2\}(\mathbf{L1})_2]_n$ featuring dinuclear $\{Cu_2(\mu_2\text{-}I)_2\}$ rhomboids were also obtained independently by control of the reaction conditions. These two CPs convert into **CP3** in hot PrCN thus indicating that this latter material is the thermodynamic product. While **CP1** and **CP2** are not emissive, **CP3** exhibits an intense luminescence due to the incorporation of the octanuclear Cu_8I_8 clusters as secondary building units (SBUs) within the network. The photophysical properties of **CP3** have been investigated and rationalized by means of DFT and TDDFT computing. Furthermore, the thermal stability of these materials has been studied by ATG and DSC analyses. The Raman spectra of **CP1-3** have been recorded in the solid state in the 50 – 500 cm^{-1} region.

INTRODUCTION

The design of coordination polymers with a predictable secondary building unit (SBU) and dimensionality is a quasi-impossible task but the quest remains of great interest for the discovery of new materials with desired properties such as gas adsorption,[1-9] sensing,[10-15] thermo-chromism,[16-19] magnetism,[20-24] conductivity,[25-28] redox-activity,[29, 30] catalysis,[13, 31-33] nonlinear optical behavior[34, 35] and luminescence.[8, 36-40] Recent reviews on CPs formed by mono- and dithioethers with CuX salts (X = Cl, Br, I)[41-47] revealed that when X = I, the SBU had a strong tendency to form closed cubanes (Cu_4I_4) and 1D staircase polymeric structures, whereas the rhomboid $Cu_2X_2S_4$ SBU is predominately noted when X = Cl or Br. The key property is that the cubanes show luminescence regardless of the ligand whereas the rhomboids and staircase motifs are almost always weakly or not emissive.[41, 44, 45] Also, the presence of 2D and 3D CPs increases drastically when semi-rigid or rigid dithioethers are used as assembling ligands.[41, 44, 45] The interest in 2D and 3D CPs stems from the possibility to form MOF-like materials.[48] Based on these statistics, one can expect to form emissive cubane-containing 2D or 3D CPs when using X = I and L = rigid dithioether. This hypothesis was recently tested by one of us by reacting CuI with trans-$Pt(PMe_3)_2(C{\equiv}CC_6H_4SMe)_2$, [Pt], leading to a porous emissive 2D CP, $(Cu_4I_4([Pt]))_n$, where the SBU is a staircase tetramer (*i.e.* completely open cubane).[49, 50] The CP exhibits a grid structure with small guests in the cavities (MeOH, MeCN, CO_2…). These reviews[41, 44, 45] also indicated the particularly rare occurrence of Cu_8I_8 clusters called fused dicubanes which account for < 5 % of all thioether/cubane-containing materials (top left, Chart 1). Considering all fused neutral dicubanes reported in the literature (only 12 cases regardless the nature of the ligand), two common features appear. Most of them are included within 2D or 3D networks and are built with rigid, specifically DABCO (1,4-diazabicyclo[2.2.2]octane), or semi-rigid ligands, and are emissive.[51-58] However, exceptions exist. Two 0D complexes employ the monodentate ligands $PPh_2(C_6H_4NMe_2)$ and $S(i\text{-}Pr)_2$,[59, 60] and for two other cases, the CPs use the flexible *p*-$TolS(CH_2)_8STol$-*p* ligand.[61, 62] Other motifs for neutral Cu_8X_8 clusters (X = Cl, Br, I; Chart 1) exist but are scarce. Indeed, only four cases are noted: a staircase octamer linked by a tetraphosphine ligand (0D),[63] a corner-shared fused cubanes driven by the small N-N bite distance of dimethyl-2,2'-biimidazole (1D),[64] an expanded hexagonal prism (*i.e.* double side-shared fused cubanes, 2D),[65] and dicoordinated hexagonal prism (3D).[66] No luminescence data have been reported for these species. Using these observations, one can anticipate that an

emissive CP of 2D or 3D dimensionality and side-shared fused cubanes used as SBUs can be formed when CuI reacts with a dithioether sharing a certain structural similarity with DABCO.

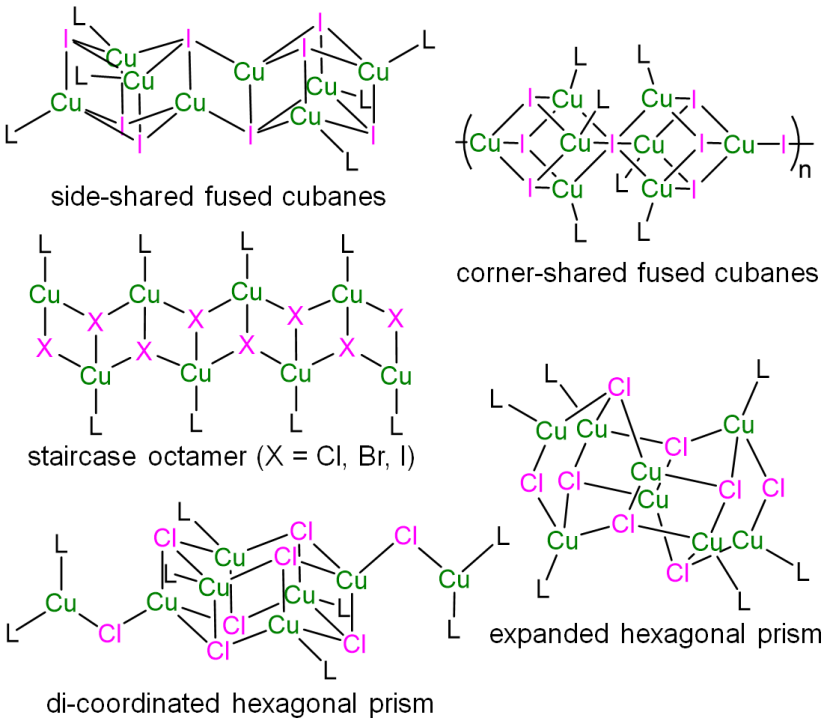

Chart 1. Structures of all encountered $Cu_8X_8L_n$ clusters in 0-, 1-, 2-, and 3D materials (X = Cl, Br, I; n = 6 (left), 8 (right); L = N, O, S, P, or C≡C-donor).

We and others have recently investigated the coordination of the short-bite dithioether ligand $ArSCH_2SAr$ with CuI and isolated a large series of 1D CPs or macrocyclic systems incorporating invariably Cu_4I_4 cubane cluster as SBUs, regardless of the substitution pattern of the Ar group. [67, 68] One possibility to further enhance the rigidity of a given dithioether is the use ligand having a cyclic framework such as 1,3-dithiane. Keller and Knaust reacted $[Cu(MeCN)_4]BF_4$ with this six-membered thiaheterocycle and obtained four coordination networks depending on metal-to-ligand ratio and solvent conditions used.[69] We report herein the coordination chemistry of the related ligand 2-methyl-1,3-dithiane, **L1**, combining both rigidity due to cyclic nature and enhanced basicity of the *S*-donor sites compared to $ArSCH_2SAr$.[67, 68] We now report that this choice of the ligand gives indeed rises to several CPs ranging from 1D-to-3D, whose architectures can be controlled by the proper reaction conditions. A rather important new feature is the observation of

a strongly luminescent CP exhibiting an unprecedented Cu_8I_8 cluster as SBU built upon two side-fused open cubanes, whose photophysical properties have been thoroughly investigated. The nature of the emissive state has been addressed using DFT and TD-DFT computations. Attempts to convert the open dicubane SBUs into closed dicubanes where not successful, where only decomposition into γ-CuI was observed.

EXPERIMENTAL SECTION

Materials and Methods. Reactions were performed using Schlenk techniques. 2-methyl-1,3-dithiane (98%, Alfa Aesar), CuI (Fischer) and proprionitrile (ACROS) were purchased and used as received. Dry CH_3CN was purified using a PureSolve MD5 system from Innovative Technology. The samples for powder XRD measurements were mixed with a small amount of paratone oil, cut to approximately 0.3 × 0.3 × 0.3 mm^3, and placed on a sample holder mounted at 173.2 K on a Bruker APEX DUO X-ray diffractometer. Six correlated runs per sample with Phi Scan of 360 degrees and exposure times of 270 s were collected with the Cu micro-focus anode (1.54184 Å) and the CCD APEX II detector at a 150 mm distance. These runs, from −12 to −72°2θ and 6 to 36ω, were then treated and integrated with the XRW2 Eval Bruker software to produce WAXD diffraction patterns from 2.5 to 82°2θ. The patterns were treated with Diffrac.Eva version 2.0 from Bruker. The thermal analysis (TGA) traces were measured on a Perkin Elmer TGA 7 apparatus in the temperature range between 25 and 950 °C at a scanning rate of 10°C.min^{-1} under argon atmosphere. The differential scanning calorimetry (DSC) plots were measured on a DSC Q200 instrument equipped with a cooling system RCS 90 both from TA instrument at a scanning rate of 10°C.min^{-1}. The IR spectra were recorded with a 2 cm^{-1} resolution on a Bruker vertex70 FTIR spectrometer using of a Platinum ATR accessory equipped with a diamond crystal. The FT-Raman spectra were recorded at 5 cm^{-1} resolution using a Bruker RFS 100/S spectrometer with the 1064 nm excitation and a light power equal to 250 mW equipped with a photomultiplier Ge-diode, cooled at liquid nitrogen temperature (77K). The peak centered between 83 and 85 cm^{-1} is considered as residual artefact from the instrument and shouldn't be considered. The solid-state UV-visible spectra were recorded on a Varian Cary 300 Bio UV-Vis spectrophotometer at 298 K using raised-angle transmittance apparatus and a homemade 77 K sample-holder. Solid-State emission, excitation, lifetimes and CIE 1931 charts

(chromaticity coordinates) were acquired on a phosphorimeter FLS980 from Edinburgh Instruments equipped with single monochromators. Samples were introduced in a capillary and spectra obtained were corrected for instrument response. The emission lifetime measurements were performed using a "flash" pulsed lamp. Lifetimes values were obtained using a time correlated single photon counting (TCSPC) system and data were treated from both deconvolution of multi-exponential analysis and exponential series method. Solid State emission quantum yields were recorded using a Quanta-φ F-3029 integration sphere from Horiba plugged into a Horiba Fluorolog III.

DFT calculations. All density functional theory (DFT) and time-dependent (TDDFT) calculations were performed with Gaussian 09[70] at the Université de Sherbrooke with the Mammouth supercomputer supported by *Le Réseau Québécois De Calculs Hautes Performances*. The DFT calculations[71-80] were carried out using the B3LYP method. A 6-31g* basis set was used for C, H and S atoms.[81-87] VDZ (valence double ζ) with SBKJC effective core potentials were used for all Cu and I. The TDDFT analysis were carried out directly on *.cif files without any optimisation.

X-ray crystallography. Single crystals of **CP1**, **CP2** and **CP3** were mounted on a Bruker D8 Venture four-circle diffractometer equipped with a nitrogen jet stream low temperature system (Oxford Cryosystems). The X-ray source was graphite monochromated Mo-Kα radiation (λ = 0.71073 Å) from a microfocus sealed tube IμS by Inocatec. Data collections have been carried out at 100 K in the case of **CP1** and **CP2**, in the case of **CP3** data were collected at five different temperatures: 100, 150, 200, 250 and 300 K, using the same crystal. The lattice parameters were obtained by least-squares fit to the optimized setting angles of the entire set of collected reflections. Intensity data were recorded as ϕ and ω scans with κ offsets. No significant intensity decay or temperature drift was observed during data collections. Data were reduced by using SAINT v8.37A (Bruker, 2015) software and absorption correction was carried out by SADABS-2016/2 (Bruker, 2016). The structure was solved using SHELXT (Sheldrick, 2015) with intrinsic phasing. Refinements were carried out by full-matrix least-squares on F2 using SHELXL program (Sheldrick, 2015) on the complete set of reflections.2 All non–hydrogen atoms were refined with anisotropic thermal parameters, whereas the H atoms were treated in a riding mode. *X-ray analysis at 350 and 400 K.* A prism-like crystal of **CP3** of approximate dimensions 0.116 x 0.163 x 0.180 mm^3, was mounted for the X-ray analysis. The X-ray intensity data were measured on a

Bruker Kappa APEX II DUO CCD system equipped with a TRIUMPH curved-crystal monochromator and a Mo fine-focus tube (λ = 0.71073 Å). The total exposure time was 4.41 hr. The frames were integrated with the Bruker SAINT software package using a narrow-frame algorithm. The integration of the data using a mono-clinic unit cell yielded a total of 24264 reflections to a maximum θ angle of 26.79° (0.79 Å resolution), of which 4947 were independent (average redundancy 4.905, completeness = 99.1%, R_{int} = 9.49%, R_{sig} = 7.98%) and 3317 (67.05%) were greater than $2\sigma(F^2)$. The final cell constants of a = 11.6059(10) Å, b = 12.8056(11) Å, c = 15.7394(13) Å, β = 90.893(4)°, volume = 2338.9(3) $Å^3$, are based upon the refinement of the XYZ-centroids of 9974 reflections above 20 σ(I) with 4.735° < 2θ < 52.90°. Data were corrected for absorption effects using the multi-scan method (SADABS). The ratio of minimum to maximum apparent transmission was 0.541. The calculated minimum and maximum transmission coefficients (based on crystal size) are 0.2880 and 0.4140. The structure was solved and refined using the Bruker SHELXTL Software Package, using the space group P1 21/c 1, with Z = 4 for the formula unit, $C_{10}H_{20}Cu_4I_4S_4$. The final anisotropic full-matrix least-squares refinement on F^2 with 202 variables converged at R1 = 6.75%, for the observed data and wR2 = 20.94% for all data. The X-ray data are placed in Tables S1 and S2.

Synthesis of CP1: To a solution of 2-methyl-1,3-dithiane (0.3 mL, 2.5 mmol) in 5 mL of acetonitrile was added an acetonitrile solution of CuI (345 mg, 1.81 mmol) (40 mL). A white precipitate appeared within 5 min. The mixture was stirred for 3 h to complete the reaction. The precipitate was filtered, washed with 2 × 30 mL acetonitrile and dried to give **CP1** as a white solid (363 mg, 62%). IR (ATR): 2952 w, 2935 w, 2904 w, 1449 w, 1422 s, 1405 m, 1375 w, 1178 w, 1162 w, 1122 m, 1074 m, 1047 m, 998 w, 904 s, 873 m, 707 m, 663 s. Anal. Calc for $C_5H_{10}CuIS_2$ (324.69): %C 18.49, %H 3.10, %S 19.75; found %C 19.77, %H 3.30, %S 20.55.

Synthesis of CP2: To an acetonitrile solution of CuI (345 mg, 1.81 mmol) (40 mL) was added neat 2-methyl-1,3-dithiane (0.3 mL, 2.5 mmol). A white precipitate appeared within 5 min. The mixture was stirred for 3 h to complete the reaction. The precipitate was filtered, washed with 2 × 30 mL acetonitrile and dried to give **CP2** as a white solid (372 mg, 63%) IR (ATR):2935 w, 2902 w, 1448 w, 1421 s, 1407 s, 1368 m, 1232 s, 1170 m, 1115 m, 1055 s, 907 s, 870 m, 819 m, 712 m, 669 s, 490 m. Anal. Calc for $C_5H_{10}CuIS_2$ (324.69): %C 18.49, %H 3.10, %S 19.75; found %C 19.02, %H 3.24, %S 20.65.

Synthesis of CP3: To solution of CuI in slight excess (478 mg, 2.5 mmol) in proprionitrile (50 mL) was added **L1** (134 mg = 0.12 mL, 1.0 mmol). A white precipitate was formed within 5 min. The suspension was stirred for additional 30 min and heated under reflux for 3h to dissolve most of the precipitate. After, the solution was allowed to cool slowly to room temperature, an homogenous microcystalline material precipitated. During the course of several days, crystals suitable for X-ray analysis appeared as small blocks. An addition, a crop of **CP3** was collected after filtering off the solid and while storing the EtCN solution in a refridgerator. Overall yield: 434 mg, 84%. IR (ATR):2954 w, 2898 w, 2878 w, 1439 w, 1417 s, 1404 s, 1371 m, 1232 s, 1195 m, 1172 m, 1055 s, 905 s, 865 m, 815 m, 712 m, 484 m. Anal. Calc for $C_{10}H_{20}Cu_4I_4S_4$ (1030.26): %C 11.66, %H 1.96, %S 12.45; found %C 11.96, %H 2.05, %S 12.85.

RESULTS AND DISCUSSION

First, **L1** was reacted with one equimolar amount of CuI in MeCN solution. A quasi-quantitative precipitation of a colorless sparingly soluble white product readily occurred. The elemental analysis indicated a 1:1 Cu/**L1** composition $[\{Cu(\mu_2\text{-}I)_2Cu\}(\mu_2\text{-}\mathbf{L1})_2]_n$. Crystals suitable for X-ray diffraction analysis were obtained by dissolving a small amount of this white product in boiling propionitrile and then allowing the crystals to form slowly (Scheme 1). Unexpectedly, two types of crystals with different shapes were detected under a microscope. First, the major fraction consisted of needle-shaped colorless crystals and crystallography analyses revealed the presence of simple 1D ribbons $[\{Cu(\mu_2\text{-}I)_2Cu\}(\mu_2\text{-}\mathbf{L1})_2]_n$ **CP1**, in which centrosymmetric dinuclear $Cu(\mu_2\text{-}I)_2Cu$ rhomboids are spanned by linking **L1** ligands (Figure 1). Although this structural motif is quite common and has been encountered for other 1D CPs described by our groups such as $[\{Cu(\mu_2\text{-}I)_2Cu\}_2\{\mu\text{-}PhS(CH_2)_5SPh\}_2]_n$, the very loose Cu···Cu contact of **CP1** reaching 3.367 Å deserves some comments. This extreme value exceeds even the long Cu···Cu separation of 3.18 Å reported for the 2D material $[(Cu_2I_2)(dtpcp)_2\bullet thf)]_n$ (dtpcp = 2,11-dithia[3.3]paracyclophane).[88] Concurrently, there are examples with short Cu–Cu bonds given by a dithioether-functionalized tetrathiafulvalene Cu(I) complex with a separation of 2.65 Å and a 1D polymer $[(Me_2S)_2\{Cu_2(\mu_2\text{-}I)_2\}]_n$, in which the metal centers within the rhomboid cluster are separated by 2.684(1) Å.[89, 90] In contrast to **CP1**, the $[\{Cu(\mu_2\text{-}I)_2Cu\}$ SBUs in the 1D CP $[\{Cu(\mu_2\text{-}I)_2Cu\}(1,2\text{-dithiane})_2]_n$ adopt an horizontally aligned orientation, with a quite short Cu–Cu distance of 2.6843(18) Å.[91] A

representative example for a CP exhibiting medium range Cu···Cu separation (2.8058(11) Å) is the 1D CP $[\{Cu(\mu_2\text{-}I)_2Cu\}_2\{\mu\text{-}PhS(CH_2)_5SPh\}_2]_n$.[92] This broad range of Cu···Cu separations underpins the structural flexibility of the $Cu(\mu_2\text{-}I)_2Cu$ motif.

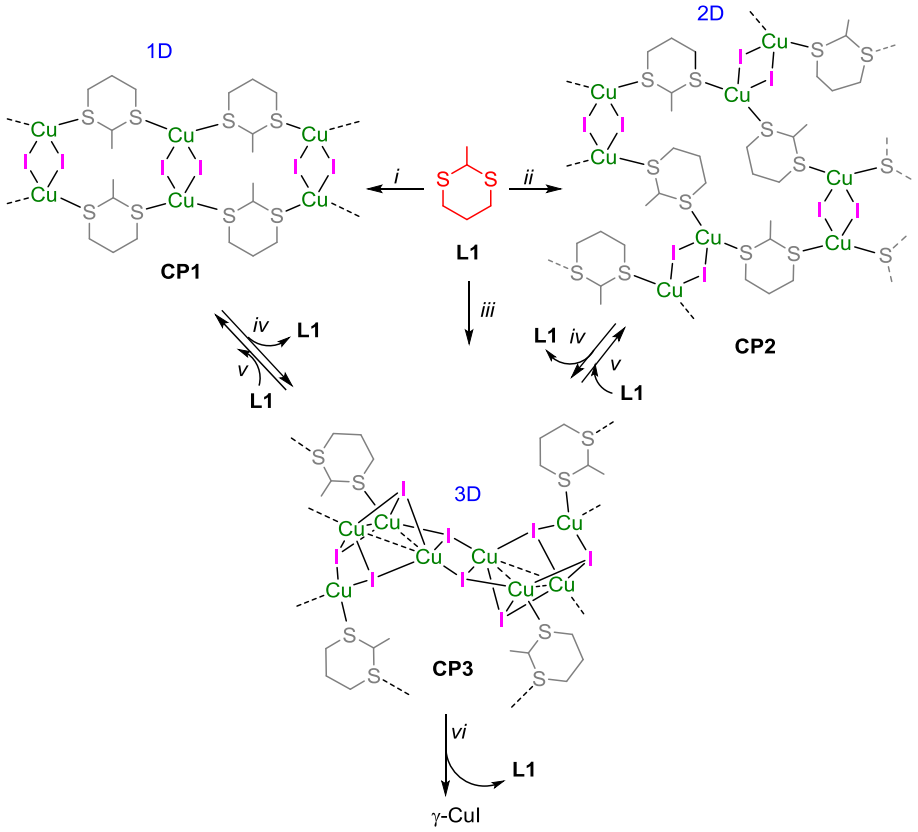

Scheme 1. Synthesis of **CP1** to **CP3**: *i*) 1:1 CuI in **L1**/MeCN RT, *ii*) 1:1 **L1** in CuI/MeCN RT, *iii*) 2:1 CuI in **L1**/EtCN reflux, *iv*) PrCN, reflux, *v*) 1Eq. **L1** *vi*) T = 170 °C.

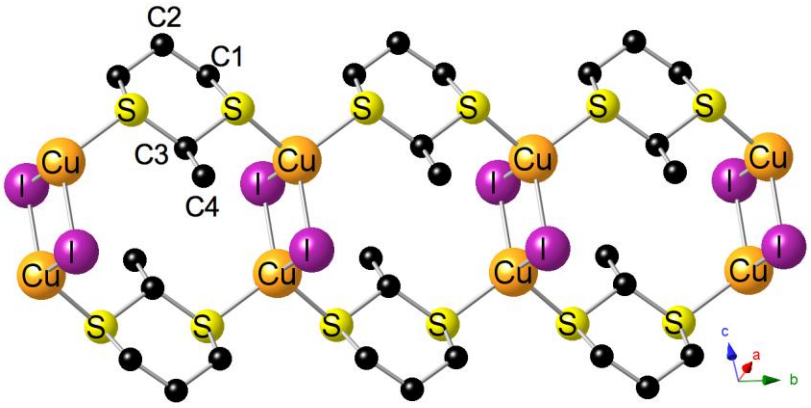

Figure 1. View of a segment of the 1D ribbon of $[\{Cu(\mu_2\text{-}I)_2Cu\}((\mu_2\text{-}\mathbf{L1})_2]_n$ **CP1** running along the *b* axis. Selected bond lengths (Å) and angles (°): Cu···Cu# 3.367, Cu–I 2.6061(3), Cu–I#

2.6834(4), Cu#–I 2.6835(4), Cu–S 2.3316(4), Cu–I–Cu# 79.042(10), I–Cu–I# 100.958(10), S–Cu–I 117.461(12), S–Cu–I# 108.487(13), S–Cu–S# 103.58(2). Symmetry transformations used to generate equivalent atoms: #1 1-x, -y, 1-z #2 +x, -y, +z #3 +x, -y, +z.

CP2 is prepared by adding **L1** to an acetonitrile solution of CuI in 1:1 Cu/**L1** ratio at room temperature. Crystals were obtained from slow evaporation of a acetonitrile solution. X-ray analysis the crystals stemming from the minor fraction revealed that **CP2** is an isomeric form of **CP1**, which differ by the connectivity of the sulfur atoms with the Cu atoms, giving rise to a 2D network (Figure 2).

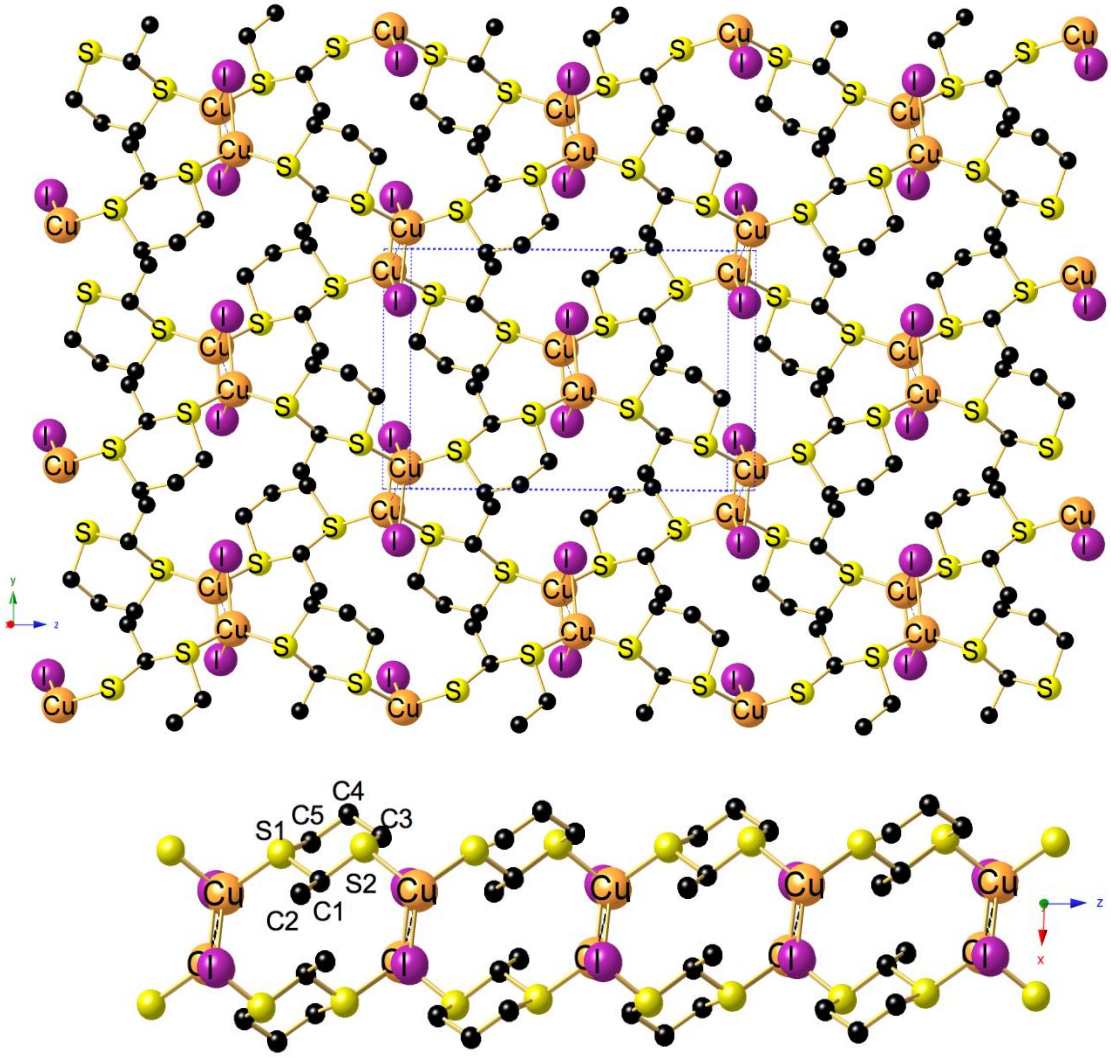

Figure 2. (Top) View on the *y,z* plane of the 2D network of $[\{Cu(\mu_2\text{-}I)_2Cu\}(\mu_2\text{-}\mathbf{L2})_2]_n$ **CP2**. Selected bond lengths (Å) and angles (°): Cu···Cu# 2.7664(6), Cu–I 2.6162(5), Cu–I#

2.6348(4), Cu#–I 2.6348(4), Cu–S1 2.3195(6), Cu–S2 2.3606(6), I–Cu–I# 116.418(11), I–Cu–Cu# 58.537(14), I#–Cu–Cu# 57.882(11), S1–Cu–I 118.275(18), S1–Cu–I# 108.194(17), S1–Cu–S2 98.51(2), S2–Cu–I 107.993(18), S2–Cu–I# 105.133(17) Symmetry transformations used to generate equivalent atoms: #1 1-x,1-y,1-z #2 +x,1/2-y,-1/2+z #3 +x,1/2-y,1/2+z. (Bottom) View down the *y* axis on a segment of a layer of **CP2** running along the *z* axis.

In this case, the SBUs are again constituted of dinuclear Cu($(\mu_2$-I$)_2$Cu rhomboids, which are spanned by both sulfur atoms of **L1**, thus forming 20-membered macrocycles in the layer. But in contrast to the 1D isomer **CP1** possessing just one type of crystallographically equivalent S atoms, the Cu atoms of the 2D isomer are ligated datively by two crystallographically different S atoms with Cu–S1 and Cu–S2 bond lengths of 2.3195(6) and 2.3606(6) Å, respectively. Another marked difference is the much closer Cu···Cu contact of 2.7664(6) Å, indicating at least a weak intermetallic interaction. This network topology is quite reminiscent to that of 2D material [{Cu(μ_2-I$)_2$Cu}(μ_2-1,3-dithiolane$)_2]_n$ resulting from the coordination of 1,3-dithiolane to CuI, and featuring a Cu···Cu distances of 2.8743(5) Å at 100 K.[39] Other similar 2D grids have previously been obtained from the reaction of CuI with the open-chain dithioethers 1,3-bis(phenylthio)propane and 1,3-bis(phenylthio)ethane respectively yielding [{Cu(μ_2-I$)_2$Cu$\}_2${μ-PhS$(CH_2)_3$SPh$\}_2]_n$ and [{Cu(μ_2-I$)_2$Cu$\}_2${μ-PhS$(CH_2)_2$SPh$\}_2]_n$.[92, 93]

CP1 and **CP2** can be therefore considered as topological isomers of formula [{Cu$_2$(μ_2-I$)_2$}(μ_2-**L1**$)_2]_n$ having the same 1:1 metal-to-ligand ratio, but different dimensionalities. Another example of topological isomerism in coordination polymers has been described by Champness, Hanton *et al*. This group has shown that three CPs of composition $[(CuI)_2(bpds)]_n$ are formed between CuI and bpds [bpds = bis(4-pyridyl)disulfide] depending upon the solvent used in crystallization and concludes that there are only minor energy differences in the formation.[94]

In order to control in a more selective manner the dimensionality of the materials, we added a MeCN solution of CuI to a MeCN solution of **L1**. This procedure yielded **CP1** in high purity as checked by PXRD (Figure 3). Inversely, **CP2** could be isolated as principal isomer by dropping **L1** at ambient temperature to a solution of CuI in MeCN (Scheme 1). Again, the purity of the phase could be ascertained by comparison of the calculated and experimental PXRD spectra with those obtained from single X-ray analysis (Figure 3).

The outcome of the reaction is furthermore impacted by the metal-to-ligand ratio. Addition of neat **L1** into an EtCN solution containing 2 equiv. of CuI led to the 3D CP $[\{Cu_8(\mu_3\text{-}I)_8\}(\mu_2\text{-}\mathbf{L1})_4]_n$, **CP3**. This yellowish air-stable luminescent material featuring octanuclear Cu_8I_8 clusters as SBUs (based on X-ray crystallography below) was formed as sole product, for which the homogeneity of the phase was ascertained by PXRD measurements (Fig. S3 SI).

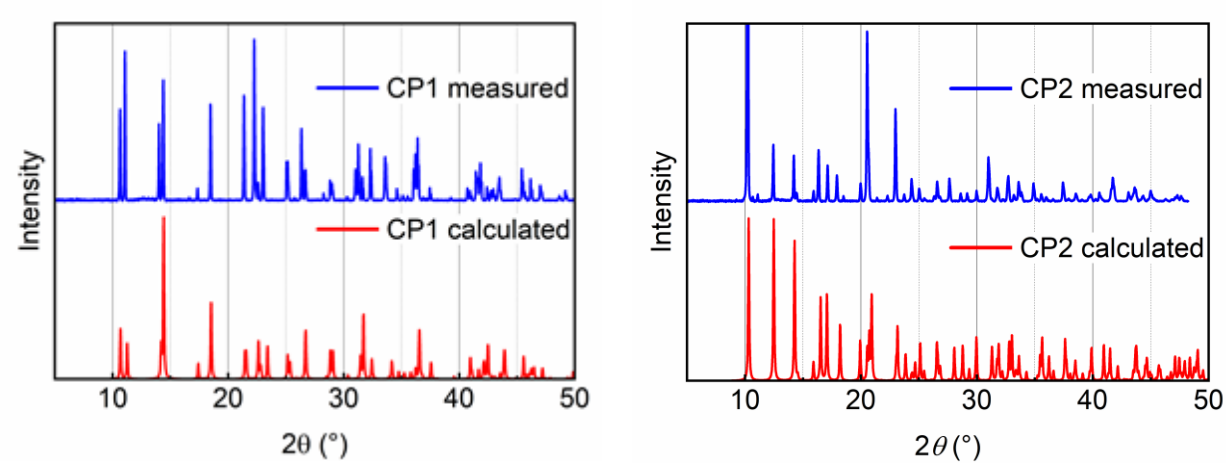

Figure 3. Comparison of experimental (red) and calculated (blue) PXRD patterns for **CP1** and **CP2**.

The X-ray data revealed that **CP3** exhibits an unprecedented motif; a side shared fused open dicubane $Cu_8I_8L_8$. This cluster differs from its homologous closed dicubane by *n* the number of ligands binding the Cu_8I_8 clusters in $Cu_8X_8L_n$. The centrosymmetric cluster core (C_i point group) shown in Figure 4 consists of two Cu1–Cu3–Cu4 triangles with a mean *d*(Cu–Cu) of 2.7069(4) Å), which is below the sum of the Van der Waals radii of two Cu atoms (2.8 Å). Each triangle is μ_3-capped by an I4 ligand. The fourth Cu2 atom is linked to Cu1 through the μ_3-bridging I1 and I2 atoms with Cu···Cu distance of 2.9184(4) Å. This motif may thus be described as a derivative of the widespread closed Cu_4I_4 cubane,[38, 39, 60-62, 67, 68, 95-97] in which two Cu–Cu bonds (per cubane) have been disconnected.

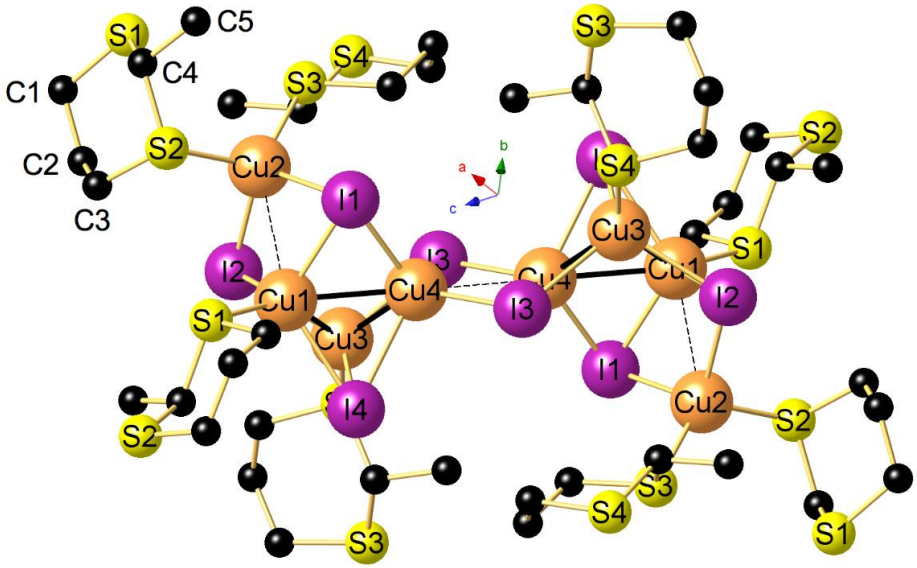
S1
C5
C4
C1
S3
S4
S2
C2
Cu2
I1
C3
I2
I3
Cu1
Cu4
S1
Cu3
I4
S2
S3
S3
S4
S2
Cu3
S1
I2
I3
I1
Cu2
S2
S3
S4
S1

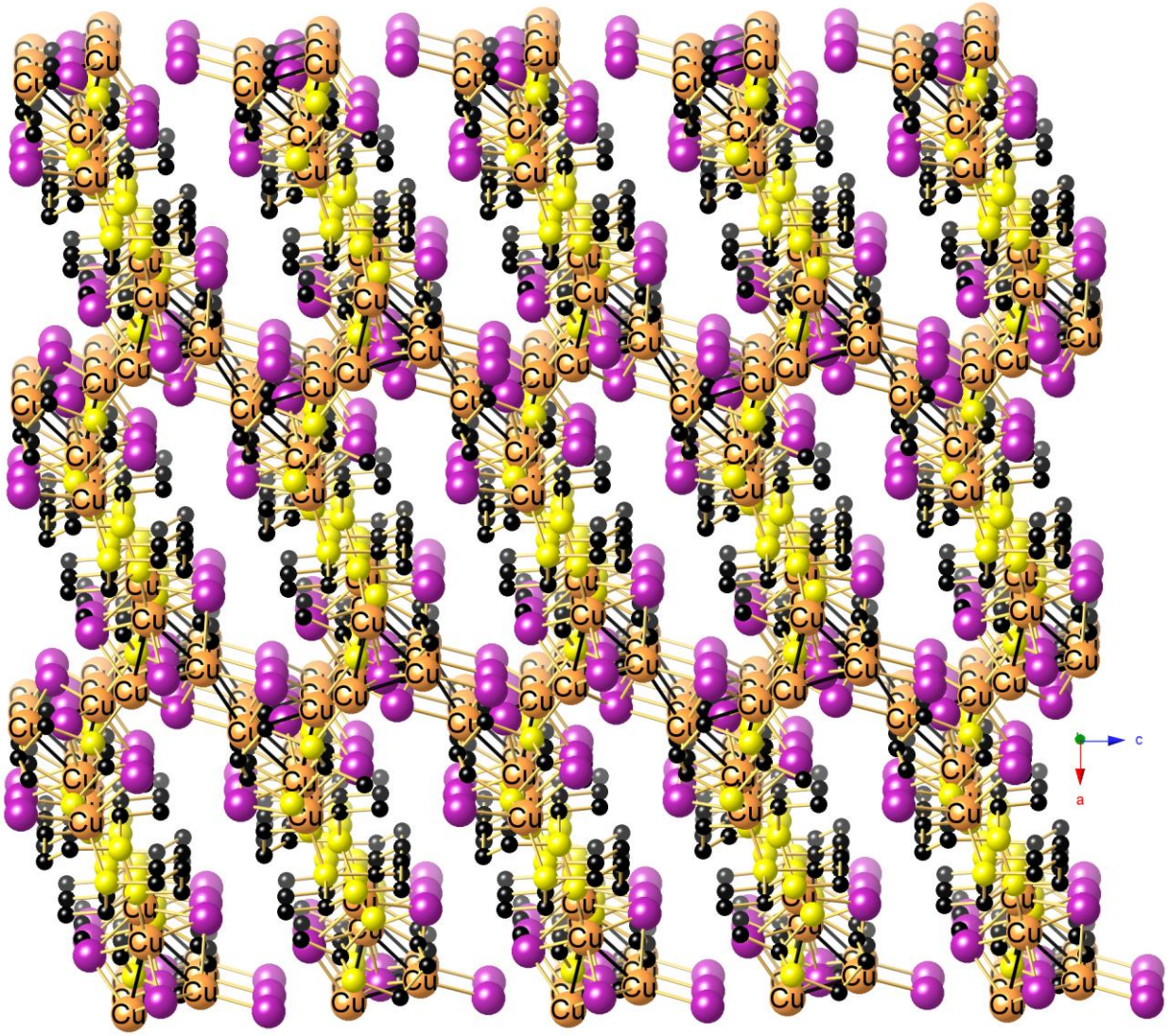
Cu
c
a

Figure 4. (Top) View of the Cu_8I_8 SBU with its ligated **L1**'s. Hydrogen atoms are omitted for clarity. Selected bond lengths (Å) and angles (°) at 100 K: Cu1–I4 2.6832(4), Cu1–I1 2.6445(5), Cu1–S1 2.3232(6), Cu2–S2 2.3010(6), Cu2–S3 2.3098(6), Cu3–S4 2.3117(6), Cu4–I3 2.6579(5), S1–S2 3.0263(7), S3–S4 2.9996(7); Cu4–I3–Cu4 67.245(13), S2–Cu2–S3 119.435(17), I3–Cu3–I2 108.356(14), Cu1–I1-Cu4–61.654(11), Cu2–I2-Cu1 66.697(13), S1–C#-S2 112.59(9), S3–C#–S4 110.80(9). Symmetry transformations used to generate equivalent atoms: #1 -1+x,+y,+z #2 1-x,-1/2+y,3/2-z #3 1-x,1-y,1-z #4 1-x,1/2+y,3/2-z #5 2-x,1-y,1-z #6 1+x,+y,+z. (Bottom) Perspective view down the *b* axis of the 3D network of **CP3**. A perspective view down the *c* axis of the 3D network of **CP3** is given in ESI (Fig. S1).

This tetranuclear subunit is linked with the second one through a Cu4···Cu4 interaction and two μ_3-bridging I3 ligands. A study of the temperature dependence of the Cu···Cu distances from 100-400 K reveals that Cu4···Cu4 separation of 2.9239(5) Å at 100 K lengthens considerably to 2.985(5) Å at 400 K (Figure S2; Table S3). No phase transition occurs in this 300 K interval (monoclinic, P*21/c*), also implying that the cubanes remained opened upon cooling. Whereas the Cu1 and Cu3 atoms are ligated by one S atom of **L1**, the Cu2 atom completes it coordination sphere with two dative Cu–S bonds, the Cu4 center is surrounded by four μ_3-iodo ligands exclusively. The assembly of the non-porous 3D network is secured by the coordination of the second S atom of the eight **L1** ligands with adjacent Cu_8I_8 SBUs.

This structural difference between closed and open dicubane can also be deduced from the difference in the Raman response of **CP3** compared to those for $[Cu_8I_8(\mathbf{L2})_3(MeCN)_2]_n$ (**L2** = *p*-TolS$(CH_2)_8$STol-*p*)[62] and $Cu_8I_8(S(i\text{-}Pr)_2)_6$[60] in the 50-500 cm^{-1} window. Indeed, the characteristic ν(CuI) region (i.e. 80-150 cm^{-1})[98] exhibits a different signature (strong central peak) for **CP3** compared to that (multiple shoulders) for $[Cu_8I_8(\mathbf{L2})_3(MeCN)_2]_n$ and $Cu_8I_8(S(i\text{-}Pr)_2)_6$ (Figures 5 and S9-S13).

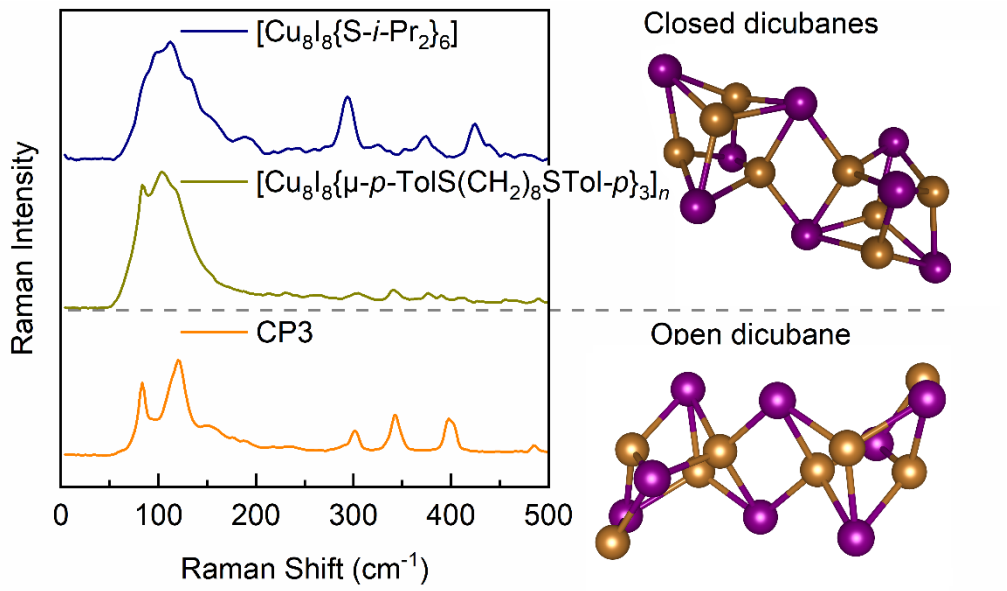

Figure 5. Solid-state FT-Raman spectra of closed and open dicubanes CPs in the 50-500 cm^{-1} region. The notch filter cutoff is 80 cm^{-1}. All Raman data for the CPs are placed in Figures S9-S13.

Interestingly, both **CP1** and **CP2** can be converted into **CP3** in refluxing PrCN indicating that **CP3** is the thermodynamic product (Scheme 1). The formation of **CP3** from **CP1** or **CP2** can be explained as such: first, when the powder is dissolved, the coordination polymer breaks in many smaller soluble fragments, a common behavior to most CPs.[99] Upon reflux in PrCN, **L1** partially dissociates and consequently the Cu/**L1** ratio increases, resembling that of the synthesis conditions to prepare **CP3**. Upon standing, crystals of **CP3** are reformed, as proven by PXRD analysis (Figure 6). Moreover, this reaction was shown to be reversible *i.e.* treatment of **CP3** with 1 equiv. of **L1** in refluxing EtCN led to a mixture of **CP1** and **CP2**. Upon the re-dissolution of **CP3**, again the CP breaks into smaller fragments, and the re-introduction of **L1** into a solution of **CP3**, **CP1** (and **CP2**) are reformed when the crystals reformed. This report of this property is, to the best of our knowledge, also unprecedented. The CP transformation from $[\{Cu_2(\mu_2\text{-}I)_2\}(\mu_2\text{-}\mathbf{L1})_2]_n$ to $[\{Cu_8(\mu_3\text{-}I)_8\}(\mu_2\text{-}\mathbf{L1})_4]_n$ is not directed by porosity change of the lattice as there is no correlation between this parameter and the nature of the CP (**CP1**, 14.8; **CP2**, 19.7; **CP3**, 16.9 %; 100 K). Instead, the cluster formation drives this process as the Cu_8I_8 unit exhibits more Cu-I bonds and Cu···Cu interactions.

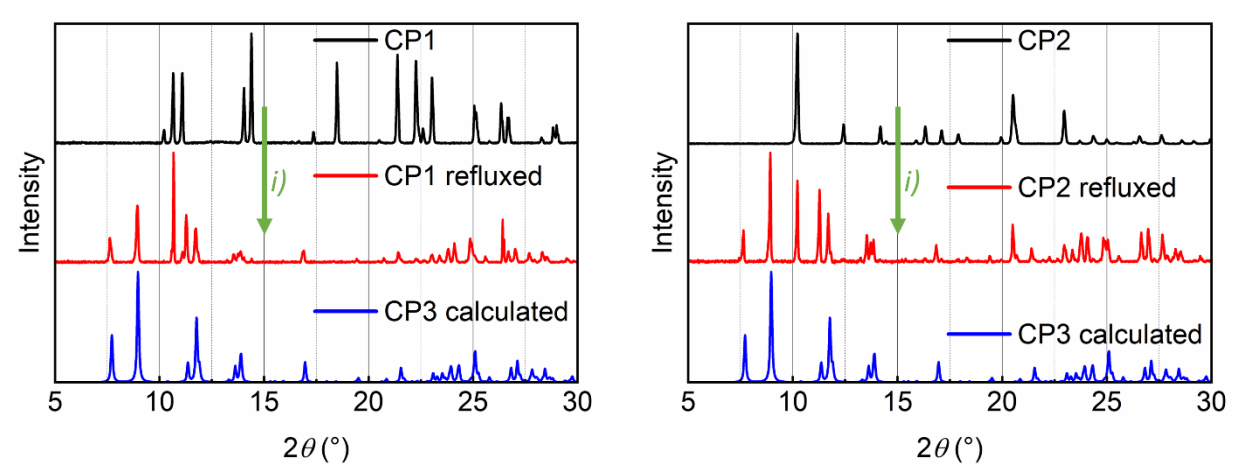

Figure 6. Powder X-ray diffraction patterns monitoring the transformation of **CP1** to **CP3** (left) and **CP2** to **CP3** (right). i) PrCN, reflux.

Thermal stabilities

The thermal stability of **CP1**, **CP2** and **CP3** was addressed by thermal gravimetric analysis (TGA) under argon up to 950°C (Figure 7; left). All CPs exhibit a similar thermal behavior where two main weight losses are readily depicted. This pattern is, in fact, typical for this type of CP.[62] The first weight loss occurs between 170-270°C. The corresponding DSC traces (Figure 7; right) revealed that, in this temperature range, three endothermic peaks are observed during the first scan, but all disappear during the next one, thus witnessing decomposition. The first weight loss corresponds to an irreversible process, that can be ascribed to a ligand loss. Based on this assumption, the experimental weight loss percent for topological isomer **CP1** and **CP2** (41 wt%) matches perfectly with the theoretical value (41 wt%) and is slightly higher for **CP3** (28 wt% vs 25 wt%; Table 1).

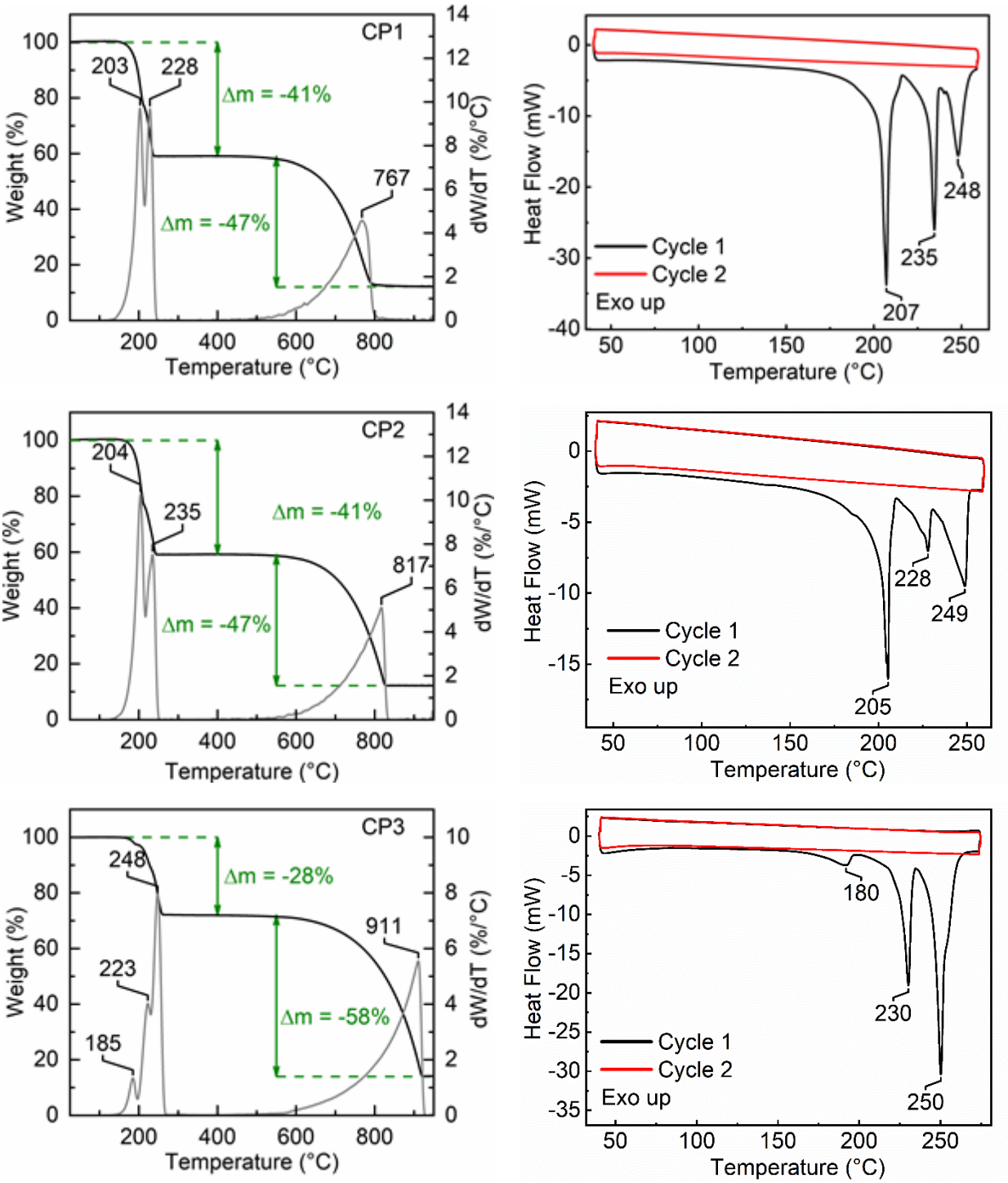

Figure 7: TGA traces (black; left) and its 1st derivative (grey; left), and DSC traces (right) of **CP1** (top) **CP2** (middle) and **CP3** (bottom) under Ar(g).

The thermal degradation temperatures that correspond to 5 wt% loss are 187 °C and 189 °C for **CP1** and **CP2** and 214 °C for **CP3**, which **c**ompared well to the values reported for other CPs

incorporating Cu_8I_8 SBUs.[62] This may be attributed to the high boiling point of the 2-methyl-1,3-dithiane ligand (bp = 224°C).

Table 1. TGA data for **CP1**, **CP2** and **CP3**

CP	T (°C)	Δm (exp) wt%	Δm (theo) wt%[a]	T_{Dec} (°C)
1	150-250	41	41	187
2	150-250	41	41	189
3	170-270	28	25	214

[a] assuming a ligand loss

Photophysical properties

CP1 and **CP2** are found non-emissive, which corroborates the trend observed in the literature.[11] However, the unprecedented motif of the Cu_8I_8 SBU urged for a detail study of the emission properties (Figure 8). Moreover, the photophysical properties of **CP3** (Table 2) were also compared to those for the 0D cluster $Cu_8I_8(S(i\text{-}Pr)_2)_6$ [60] and the CPs $[Cu_8I_8(p\text{-}TolS(CH_2)_8STol\text{-}p)_3(MeCN)_2]_n$ and $[Cu_8I_8(p\text{-}TolS(CH_2)_8STol\text{-}p)_3(EtCN)_2]_n$.[62] **CP3** is strongly luminescent (Figure S14) and exhibits a strong emission band at 534 nm which red-shifts to 574 nm upon going from 298 to 77 K (Figure 8). This low-energy emissive excited state has been previously attributed to a cluster-centered transition for both closed and open Cu_4I_4 cubanes.[62] The emission maxima λ_e at 77 K is red-shifted compared to that found for $[Cu_8I_8(p\text{-}TolS(CH_2)_8STol\text{-}p)_3(MeCN)_2]_n$ and $[Cu_8I_8(p\text{-}TolS(CH_2)_8STol\text{-}p)_3(EtCN)_2]_n$. This is fully consistent with a shorter mean *d*(Cu-Cu) distance for **CP3** (2.7139 Å at 150 K and 2.7270 Å at 200 K) compared to those for $[Cu_8I_8(p\text{-}TolS(CH_2)_8STol\text{-}p)_3(MeCN)_2]_n$ (2.7494 Å) and $[Cu_8I_8(p\text{-}TolS(CH_2)_8STol\text{-}p)_3(EtCN)_2]_n$ (2.7382Å) at 173 K. The emission maxima (λ_e), quantum yields (Φ_e) and lifetimes (τ_e) of **CP3** compare somewhat favorably to that for other Cu_8I_8-species containing thio-ligands (Table 2). The largest Φ_e value ever reported for a Cu_8I_8-cluster, regardless of the nature of the ligand, is 68 %.[57] However, the most significant difference is the larger full width at half maximum, fwhm, of the emission band (5900 cm^{-1}). This property stems from hot bands originating from thermally populated upper vibronic levels.[100] Indeed, upon cooling to 77 K, the fwhm decreases to 2900 cm^{-1} (Δfwhm = 3000 cm^{-1}). This Δfwhm is also larger than that for the closed fused dicubanes (500-1800 cm^{-1}), which is associated with the

presence of a larger number of lower-frequency Frank-Condon active modes in the open dicubane. This feature is consistent with its lower symmetry (C_i *vs*. C_{2h}) and lesser rigid skeleton.

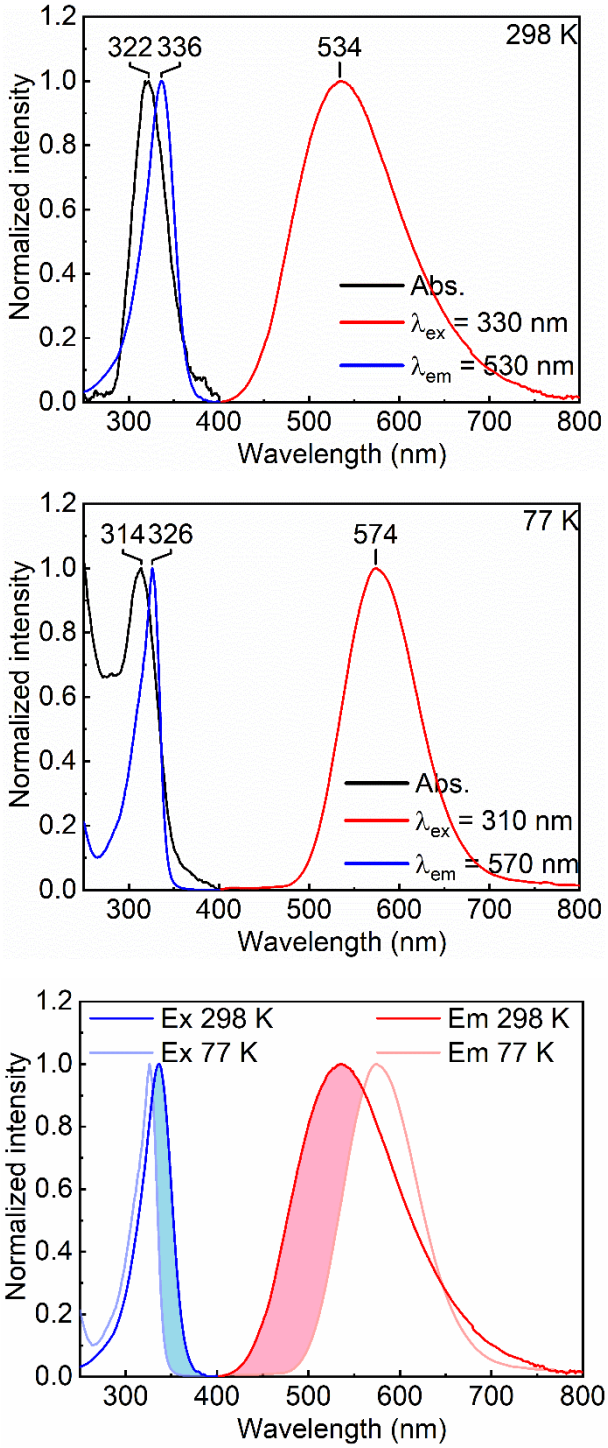

Figure 8. Solid-state emission (red) and excitation (blue) for **CP3** at 298 (top) and 77 K (middle) and their overlaps stressing the highlighted regions in color filling associated with the presence

of "hot bands". Essentially, the contribution of the hot bands is more significant in the open dicubane than that for the closed dicubane (see the Δfwhm data in Table 2 and text).

Table 2. Comparison of the photophysical data for **CP1**, **CP2**, **CP3**, **CP3** sonicated and **CP3**@200°C and literature CPs containing the closed Cu_8I_8 SBU.

CP	T (K)	λ_{em} (nm)	fwhm (cm^{-1})	Δfwhm[a] (cm^{-1})	τ_e[b] (μs)	χ^2	Φ (%)	k_r[c] (10^5 s^{-1})	k_{nr}[c] (10^5 s^{-1})
CP3	298	534	5900	3000	2.41	1.06	36	1.5	2.7
	77	574	2900		2.51	1.00	-	-	-
CP3 sonicated	298	539	4500	1800	2.04	1.11	40	1.9	3.0
	77	571	2700		1.92	1.12	-	-	-
CP3@200°C	298	541	4700	2000	1.79	0.96	19	1.0	4.5
	77	580	2700		2.13	1.13	-	-	-
$[Cu_8I_8(\mathbf{L2})_3(MeCN)_2]_n$[d]	298	530	3400	1600	2.72	-[f]	56	2.1	1.6
	77	538	1800		5.27	-[f]	-	-	-
$[Cu_8I_8(\mathbf{L2})_3(EtCN)_2]_n$[d]	298	539	3800	1800	1.09	-[f]	10	0.9	8.2
	77	551	2000		4.88	-[f]	-	-	-
$Cu_8I_8(S(i\text{-}Pr)_2)_6$ (0D)[e]	298	573	3700	500	0.20	-[f]	45	2.3	2.75
	77	532	3200		0.26	-[f]	-	-	-

[a] Δ_{fwhm} = (fwhm 298 K) – (fwhm 77 K); fwhm = full width at half maximum. [b] The emission decays and curve fittings are provided in Figures S16-S18. [c] $k_r = \frac{\Phi}{\tau_e}$; $k_{nr} = \frac{kr}{\Phi}(1-\Phi)$. [d] **L2** = *p*-TolS$(CH_2)_8$STol-*p* from ref. 62. From ref. 60. [f] Data not reported.

DFT and TDDFT calculations

The nature of the emissive excited state was addressed by DFT and TDDFT computations. The X-ray data for one $Cu_8I_8(\mathbf{L1})_4$ unit were selected for the calculations (Figures 9 and S20-21)). TDDFT places the spin-allowed lowest energy transition at 312 nm (Table 3), which compares favorably to the experimental value of 314 at 77 K, a temperature where the presence of hot bands is minimal (Figure 8). This transition is composed mainly of HOMO→LUMO (91 %). These MOs are composed of 88.6 and 11.4 % (HOMO), and 29.8 and 70.2 % (LUMO) of atomic contributions located within Cu_8I_8 and **L1**, respectively (Tables 4 and S4-S5). So, this S_1 state is

best described as metal/halide-to-ligand charge transfer (M/XLCT). Concurrently in the triplet state, the highest and lowest semi-occupied orbitals, HSOMO and LSOMO, exhibit atomic orbital contributions similar to the HOMO and LUMO, respectively, thus indicating that the emissive state is ^{3}(M/XLCT)*. This conclusion is the same as that made for the side shared fused closed dicubane version ($Cu_8I_8L_6$)[60] indicating that breaking two Cu-I bonds does not alter the nature of the lowest energy excited states.

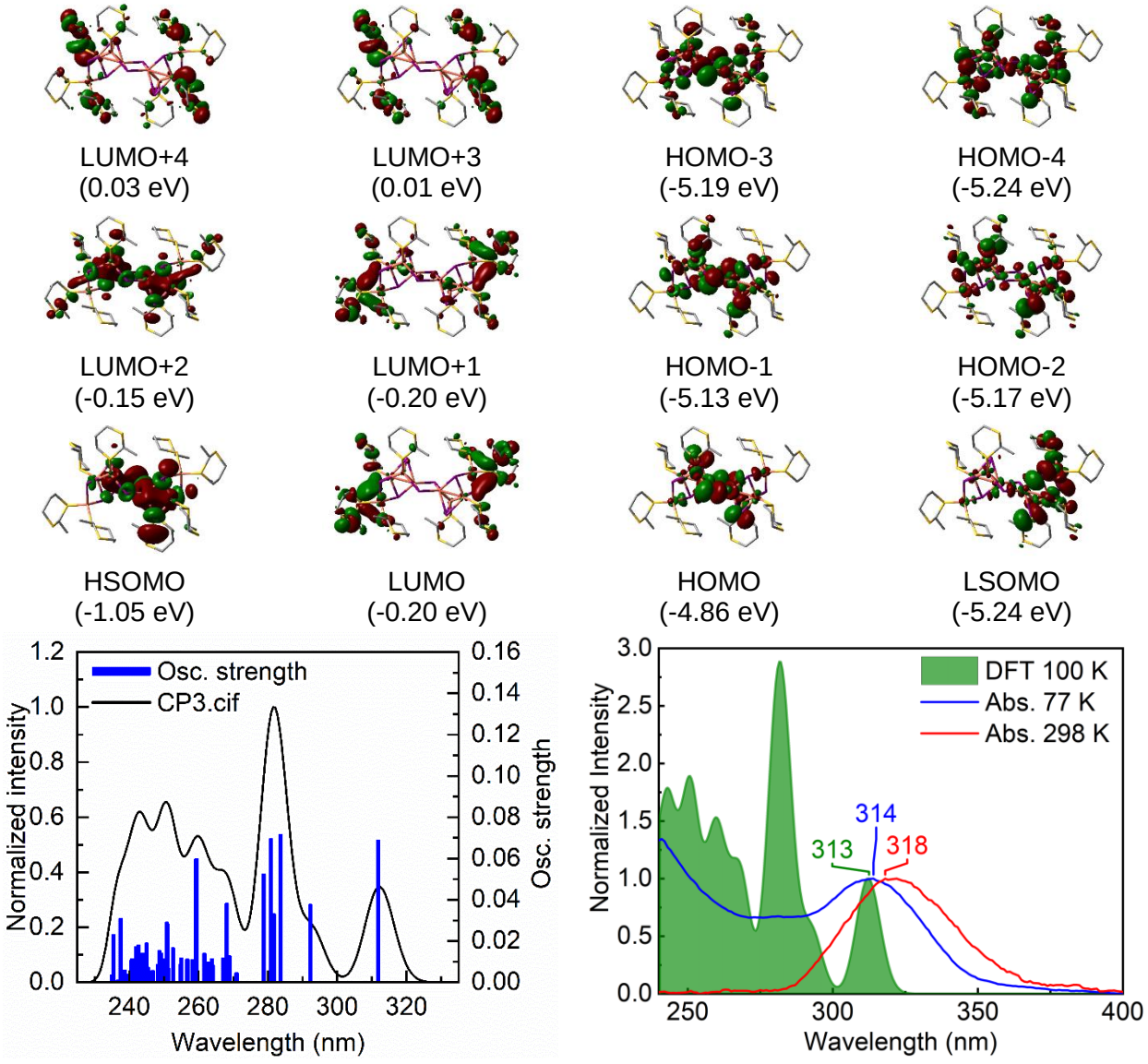

Figure 9. (Top) Representation of the frontier MOs of the Cu_8I_8 fragment in **CP3**. (Bottom) left: bar graph reporting the calculated oscillator strength (f) and calculated position of the 100st electronic transitions calculated by TDDFT for **CP3**.cif (bar graph; f *versus* λ). The black line is

generated by assigning an arbitrary thickness of 1000 cm^{-1} to each bar. (Right) Stacking of the simulated (green) and experimental solid-state absorption spectrum at 298 (red) and 77 K (blue). The position of the lowest energy transition matches favorably that for the experimental value of 314 at 77 K.

Table 3. Calculated position, oscillator strength (*f*) and major contributions of the first five singlet-singlet electronic transitions of **CP3**

λ (nm)	*f*	Major contributions (%)
311.8	0.0685	HOMO→LUMO (91)
296.5	0	HOMO→L+1 (26), HOMO→L+3 (56)
293.1	0	H-2→LUMO (68), H-1→L+3 (17)
292.2	0.0375	H-2→L+3 (21), H-1→LUMO (63)
284.1	0	HOMO→L+1 (56), HOMO→L+3 (21)

[a] The first 100 computed electronic transitions are given in the SI (Table S4)

Table 4. Atomic distributions of the frontier MOs for **CP3**.

	H-4	H-3	H-2	H-1	HOMO	LUMO	L+1	L+2	L+3	L+4
Cu_8I_8	62.1	80.9	64.7	72.5	88.6	29.8	36.8	71.4	28.2	36.9
L1	37.9	19.1	35.3	27.5	11.4	70.2	63.2	28.6	71.8	63.1

Attempt to convert CP3 into closed dicubane

This unprecedented Cu_8I_8 motif urged for a tentative conversion into its closed version. Indeed, attempts were made to convert this open dicubane into a closed one by both thermal annealing at 140 °C or by sonication of **CP3** (Figures S4 and S5). This temperature was chosen based on TGA and DSC experiments (*vide supra*) showing that **CP3** is stable up to 170°C where it starts losing the ligand. The effects of sonication and thermal annealing on **CP3** were monitored by PXRD (Figures 10 and S4-S8), emission and excitation spectra (Figures S15, S16) and lifetime measurements (Table 2, Figures S17-S19). The PXRD patterns show that the main scatterings remain intact but smaller ones either decrease upon thermal annealing and increases upon sonication when compared to the native **CP3** (Figure 10). This behavior indicates that new reflection planes are created upon sonication and removed upon heating meaning that the former

leads to fragmentation of the particles and thermal annealing fuses them. As expected, the photophysical properties vary a little (Table 2, Figures S14, S15), and the Cu_8I_8 geometry remains intact. This relative robustness is consistent with the large density of the solid (3.014 g/cm^3) compared to 2.45 for **CP1** and 2.34 g/cm^3 for **CP2** (100 K), where large crystal re-organization is readily precluded.

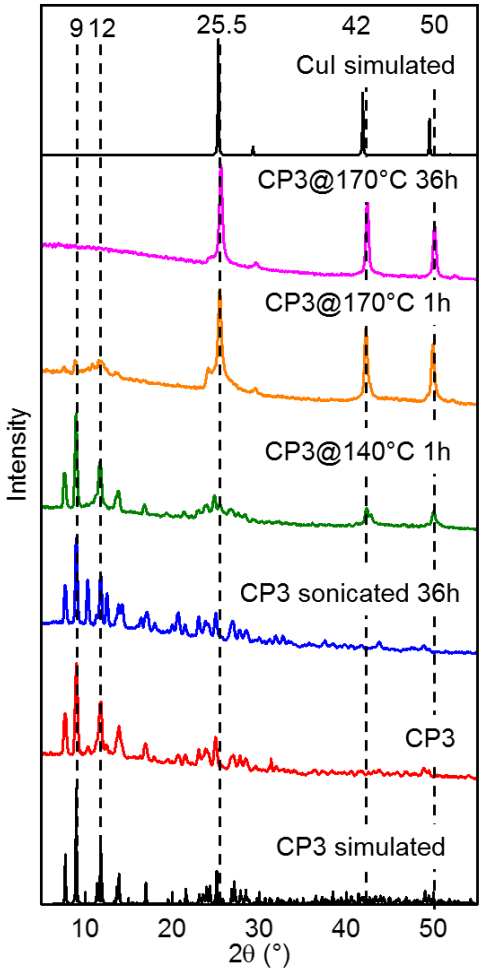

Figure 10. Monitoring of the PXRD patterns of **CP3** treated under various conditions (red = native).

Finally, upon further heating up to 170°C for 36h, the PXRD pattern (Figures S6-8) provides evidence for the formation of γ-CuI.[100] This reaction path is not unprecedented,[101] and altogether the open Cu_8I_8 dicubane could not be converted into the closed one.

CONCLUSION

The use of the CuX salt specifically where X = I, and a dithioether ligand exhibiting similar structural traits to DABCO (*i.e*. both donors are situated inside a 6-membered ring), led to the anticipated formation of a luminescent 3D CP incorporating a Cu_8I_8 SBU. The statistical approach of literature data stressed in the introduction above to predict the outcome of a CP formation appears clearly an appealing step towards their rational design. Moreover, the conversion of **CP1** and **CP2**, obtained from different routes from the same raw materials, into **CP3** indicates that **CP3** is the thermodynamic product. However, the observed reversibly **CP1↔CP3↔CP2** also indicates controlling the nature of the resulting CP. This conclusion also suggests that literature must be filled with CPs that can be further transformed. For instance, just crushing crystals may induce a structural change in both the SBU and CP dimensionality.[59] The unprecedented structure for a Cu_8X_8 cluster is herein the most interesting finding. This open dicubane differs from the closed one by the insertion of two Cu-S bonds at the cost of two Cu-I ones without altering the remainders within the cluster, resulting into an emissive species using a same ^{3}(M/XLCT)* manifold. Our open dicubane motif constitutes the "missing link" between the closed cubane-type cluster, the flower basked type Cu_4I_4 cluster featuring one broken Cu–Cu bond and the open-cubane structure. [102, 103]

Attempts to "close" the dicubane failed, which is consistent with the fact that **CP3** is the thermodynamic product and that the CP is relatively dense. Instead, heating **CP3** at T > 160 °C leads to decomposition, with the formation of γ-CuI. We are currently investigating the coordination chemistry of **L1** vis-à-vis CuBr and CuCl and the possibility to built-up luminescent material with dithiane itself and other 2-substituted dithiane derivatives.

ASSOCIATED CONTENT

Supporting Information. Crystallographic data in CIF file, summary of X-ray data collection and refinement of **CP1**, **CP2** and **CP3**, temperature-dependent bond distances for **CP3**, electronic transition energy, oscillator strength (f) and major contributions of the first 100 singlet-singlet electronic transitions TDDFT calculated for **CP3**, enlarged PXRD for **CP3** upon sonication and annealing, enlarged Raman spectra (PDF). The following files are available free of charge on the ACS publication website at hppt://pubs.acs.org.

AUTHOR INFORMATION

Corresponding Author

* Pierre.Harvey@USherbrooke.ca

* Michael.Knorr@univ-fcomte.fr

* lydie.viau@univ-fcomte.fr

Author Contributions

The manuscript was written through contributions of all authors. All authors have given approval to the final version of the manuscript.

Funding Sources

This work was supported by the Natural Sciences and Engineering Research Council of Canada, the Fonds de Recherche du Québec-Nature et Technologies, Compute Canada and Calcul Québec, the Centre Quebecois sur les Matériaux Fonctionnels and the CNRS.

REFERENCES

1. Bezuidenhout, C. X.; Esterhuysen, C.; Barbour, L. J. Solvatochromism as a probe to observe the solvent exchange process in a 1-D porous coordination polymer with 1-D solvent accessible channels. *Chem. Commun.* **2017,** *53*, 5618-5621.
2. Du, M.; Li, C.-P.; Chen, M.; Ge, Z.-W.; Wang, X.; Wang, L.; Liu, C.-S. Divergent Kinetic and Thermodynamic Hydration of a Porous Cu(II) Coordination Polymer with Exclusive CO2 Sorption Selectivity. *J. Am. Chem. Soc.* **2014,** *136*, 10906-10909.
3. Elsaidi, S. K.; Mohamed, M. H.; Wojtas, L.; Cairns, A. J.; Eddaoudi, M.; Zaworotko, M. J. Two-step crystal engineering of porous nets from $Cr_3(\mu_3\text{-}O)(RCO_2)_6$ and $Cu_3(\mu_3\text{-}Cl)(RNH_2)_6Cl_6$ molecular building blocks. *Chem. Commun.* **2013,** *49*, 8154-8156.
4. Hawes, C. S.; Babarao, R.; Hill, M. R.; White, K. F.; Abrahams, B. F.; Kruger, P. E. Hysteretic carbon dioxide sorption in a novel copper(II)-indazole-carboxylate porous coordination polymer. *Chem. Commun.* **2012,** *48*, 11558-11560.
5. Kotani, R.; Kondo, A.; Maeda, K. Gate adsorption of CO_2 on a flexible one-dimensional copper-based coordination polymer crystal. *Chem. Commun.* **2012,** *48*, 11316-11318.
6. Procopio, E. Q.; Fukushima, T.; Barea, E.; Navarro, J. A. R.; Horike, S.; Kitagawa, S. A Soft Copper(II) Porous Coordination Polymer with Unprecedented Aqua Bridge and Selective Adsorption Properties. *Chem. Eur. J.* **2012,** *18*, 13117-13125.
7. Shigematsu, A.; Yamada, T.; Kitagawa, H. Selective Separation of Water, Methanol, and Ethanol by a Porous Coordination Polymer Built with a Flexible Tetrahedral Ligand. *J. Am. Chem. Soc.* **2012,** *134*, 13145-13147.

8. Prochowicz, D.; Justyniak, I.; Kornowicz, A.; Kaczorowski, T.; Kaszkur, Z.; Lewinski, J. Construction of a Porous Homochiral Coordination Polymer with Two Types of Cu_nI_n Alternating Units Linked by Quinine: A Solvothermal and a Mechanochemical Approach. *Chem. Eur. J.* **2012,** *18*, 7367-7371.
9. Burd, S. D.; Ma, S. Q.; Perman, J. A.; Sikora, B. J.; Snurr, R. Q.; Thallapally, P. K.; Tian, J.; Wojtas, L.; Zaworotko, M. J. Highly Selective Carbon Dioxide Uptake by $Cu(bpy\text{-}n)_2(SiF_6)$ (bpy-1=4,4 '-Bipyridine; bpy-2=1,2-Bis(4-pyridyl)ethene). *J. Am. Chem. Soc.* **2012,** *134*, 3663-3666.
10. Meilikhov, M.; Furukawa, S.; Hirai, K.; Fischer, R. A.; Kitagawa, S. Binary Janus Porous Coordination Polymer Coating for Sensor Devices with Tunable Analyte Affinity. *Angew. Chem. Int. Ed.* **2013,** *52*, 341-345.
11. Varju, B. R.; Ovens, J. S.; Leznoff, D. B. Mixed Cu(I)/Au(I) coordination polymers as reversible turn-on vapoluminescent sensors for volatile thioethers. *Chem. Commun.* **2017,** *53*, 6500-6503.
12. Liu, S. Y.; Qi, X. L.; Lin, R. B.; Cheng, X. N.; Liao, P. Q.; Zhang, J. P.; Chen, X. M. Porous Cu(I) Triazolate Framework and Derived Hybrid Membrane with Exceptionally High Sensing Effi ciency for Gaseous Oxygen. *Adv. Funct. Mater.* **2014,** *24*, 5866-5872.
13. Wen, T.; Zhang, D.-X.; Liu, J.; Lin, R.; Zhang, J. A multifunctional helical Cu(I) coordination polymer with mechanochromic, sensing and photocatalytic properties. *Chem. Commun.* **2013,** *49*, 5660-5662.
14. Song, Y.; Fan, R.; Du, X.; Xing, K.; Dong, Y.; Wang, P.; Yang, Y. Dual functional fluorescent sensor for selectively detecting acetone and Fe^{3+} based on $\{Cu_2N_4\}$ substructure bridged Cu(I) coordination polymer. *RSC Adances* **2016,** *6*, 110182-110189.
15. Zhang, W.; Jin, W.; Fukushima, T.; Mori, T.; Aida, T. Helix Sense-Selective Supramolecular Polymerization Seeded by a One-Handed Helical Polymeric Assembly. *J. Am. Chem. Soc.* **2015,** *137*, 13792-13795.
16. Veselska, O.; Podbevsek, D.; Ledoux, G.; Fateeva, A.; Demessence, A. Intrinsic triple-emitting 2D copper thiolate coordination polymer as a ratiometric thermometer working over 400 K range. *Chem. Commun.* **2017,** *53*, 12225-12228.
17. Kim, T. H.; Shin, Y. W.; Jung, J. H.; Kim, J. S.; Kim, J. Crystal-to-crystal transformation between three Cu-I coordination polymers and structural evidence for luminescence thermochromism. *Angew. Chem. Int. Ed.* **2008,** *47*, 685-688.
18. Zhan, S.-Z.; Li, M.; Zhou, X.-P.; Wang, J.-H.; Yang, J.-R.; Li, D. When Cu_4I_4 cubane meets $Cu_3(pyrazolate)_3$ triangle: dynamic interplay between two classical luminophores functioning in a reversibly thermochromic coordination polymer. *Chem. Commun.* **2011,** *47*, 12441-12443.
19. Troyano, J.; Perles, J.; Amo-Ochoa, P.; Ignacio Martinez, J.; Concepcion Gimeno, M.; Fernandez-Moreira, V.; Zamora, F.; Delgado, S. Luminescent Thermochromism of 2D Coordination Polymers Based on Copper(I) Halides with 4-Hydroxythiophenol. *Chem. Eur. J.* **2016,** *22*, 18027-18035.
20. Coronado, E.; Gimenez-Marques, M.; Espallargas, G. M.; Brammer, L. Tuning the magneto-structural properties of non-porous coordination polymers by HCl chemisorption. *Nat. Commun.* **2012,** *3*, 8.
21. Zhu, M.; Yang, M.; Wang, J.; Li, H.; Li, L. Structural and Magnetic Properties of 2p-3d-4f Hetero-Tri-Spin Chains Comprising $\{Cu(hfac)_2\text{-Radical}\}_2$ Dimers and $Ln(hfac)_3$ (hfac=hexafluoroacetylacetonate). *Chem. Asian J.* **2016,** *11*, 1900-1905.

22. Amacher, A. M.; Puigmarti-Luis, J.; Geng, Y.; Lebedev, V.; Laukhin, V.; Kraemer, K.; Hauser, J.; Amabilino, D. B.; Decurtins, S.; Liu, S.-X. Coordination-directed self-assembly of a simple benzothiadiazole-fused tetrathiafulvalene to low-bandgap metallogels. *Chem. Commun.* **2015,** *51*, 15063-15066.
23. Qin, Y.-L.; Yao, R.-X.; Wu, G.-X.; Liu, M.-M.; Zhang, X.-M. Heterometallic Mixed-Valence Copper(I,II) Cyanides that were Tuned by Using the Chelate Effect: Discovery of Famous Cairo Pentagonal Tiling and Unprecedented (3,4)-Connected $\{8^3\}_2\{8^6\}$ Topological 3D Net. *Chem. Asian J.* **2013,** *8*, 1587-1595.
24. Prescimone, A.; Morien, C.; Allan, D.; Schlueter, J. A.; Tozer, S. W.; Manson, J. L.; Parsons, S.; Brechin, E. K.; Hill, S. Pressure-Driven Orbital Reorientations and Coordination-Sphere Reconstructions in $CuF_2(H_2O)_2$(pyz). *Angew. Chem. Int. Ed.* **2012,** *51*, 7490-7494.
25. Huang, X.; Zhang, S.; Liu, L. Y.; Yu, L.; Chen, G. F.; Xu, W.; Zhu, D. B. Superconductivity in a Copper(II)-Based Coordination Polymer with Perfect Kagome Structure. *Angew. Chem. Int. Ed.* **2018,** *57*, 146-150.
26. Amo-Ochoa, P.; Hassanein, K.; Gomez-Garcia, C. J.; Benmansour, S.; Perles, J.; Castillo, O.; Martinez, J. I.; Ocon, P.; Zamora, F. Reversible stimulus-responsive Cu(I) iodide pyridine coordination polymer. *Chem. Commun.* **2015,** *51*, 14306-14309.
27. Huang, X.; Sheng, P.; Tu, Z.; Zhang, F.; Wang, J.; Geng, H.; Zou, Y.; Di, C.-a.; Yi, Y.; Sun, Y.; Xu, W.; Zhu, D. A two-dimensional pi-d conjugated coordination polymer with extremely high electrical conductivity and ambipolar transport behaviour. *Nat. Commun.* **2015,** *6*.
28. Okubo, T.; Anma, H.; Tanaka, N.; Himoto, K.; Seki, S.; Saeki, A.; Maekawa, M.; Kuroda-Sowa, T. Crystal structure and carrier transport properties of a new semiconducting 2D coordination polymer with a 3,5-dimethylpiperidine dithiocarbamate ligand. *Chem. Commun.* **2013,** *49*, 4316-4318.
29. de Hatten, X.; Asil, D.; Friend, R. H.; Nitschke, J. R. Aqueous Self-Assembly of an Electroluminescent Double-Helical Metallopolymer. *J. Am. Chem. Soc.* **2012,** *134*, 19170-19178.
30. Fadaee, F.; Amirnasr, M.; Prsa, K.; Pattison, P.; Shaik, N. E.; Ronnow, H. M.; Esrafili, M. D.; Omrani, A. A.; Amiri, A.; Schenk-Joss, K. Intrachain antiferromagnetic exchange in a 1D branched-chain built of two different copper(II) centres interlinked by end-on azido and phenoxo bridges: electron density map, electrochemical and magnetic properties. *RSC Adances* **2015,** *5*, 59926-59934.
31. Wen, T.; Zhang, D.-X.; Zhang, H.-X.; Zhang, H.-B.; Zhang, J.; Li, D.-S. Redox-active Cu(I) boron imidazolate framework for mechanochromic and catalytic applications. *Chem. Commun.* **2014,** *50*, 8754-8756.
32. Zakaria, M. B.; Hu, M.; Tsujimoto, Y.; Sakka, Y.; Suzuki, N.; Kamachi, Y.; Imura, M.; Ishihara, S.; Ariga, K.; Yamauchi, Y. Controlled Crystallization of Cyano-Bridged Cu-Pt Coordination Polymers with Two-Dimensional Morphology. *Chem. Asian J.* **2014,** *9*, 1511-1514.
33. Hou, Y.-L.; Sun, R. W.-Y.; Zhou, X.-P.; Wang, J.-H.; Li, D. A copper(I)/copper(II)-salen coordination polymer as a bimetallic catalyst for three-component Strecker reactions and degradation of organic dyes. *Chem. Commun.* **2014,** *50*, 2295-2297.
34. Chen, X.; Li, H. X.; Zhang, Z. Y.; Zhao, W.; Lang, J. P.; Abrahams, B. F. Activation and amplification of the third-order NLO and luminescent responses of a precursor cluster by a supramolecular approach. *Chem. Commun.* **2012,** *48*, 4480-4482.
35. Zhang, J. F.; Jia, D.; Humphrey, M. G.; Meng, S. C.; Zaworotko, M. J.; Cifuentes, M. P.; Zhang, C. Ammonium-crown ether supramolecular cation-templated assembly of an

unprecedented heterobicluster-metal coordination polymer with enhanced NLO properties. *Chem. Commun.* **2016,** *52*, 3797-3800.
36. Gallego, A.; Hermosa, C.; Castillo, O.; Berlanga, I.; Gomez-Garcia, C. J.; Mateo-Marti, E.; Martinez, J. I.; Flores, F.; Gomez-Navarro, C.; Gomez-Herrero, J.; Delgado, S.; Zamora, F. Solvent-Induced Delamination of a Multifunctional Two Dimensional Coordination Polymer. *Adv. Mater.* **2013,** *25*, 2141-2146.
37. Wen, T.; Zhou, X.-P.; Zhang, D.-X.; Li, D. Luminescent Mechanochromic Porous Coordination Polymers. *Chem. Eur. J.* **2014,** *20*, 644-648.
38. Cho, S.; Jeon, Y.; Lee, S.; Kim, J.; Kim, T. H. Reversible Transformation between Cubane and Stairstep Cu4I4 Clusters Using Heat or Solvent Vapor. *Chem. Eur. J.* **2015,** *21*, 1439-1443.
39. Raghuvanshi, A.; Strohmann, C.; Tissot, J.-B.; Clement, S.; Mehdi, A.; Richeter, S.; Viau, L.; Knorr, M. Assembly of Coordination Polymers Using Thioether-Functionalized Octasilsesquioxanes: Occurrence of $(CuX)_n$ Clusters (X=Br and I) within 3D-POSS Networks. *Chem. Eur. J.* **2017,** *23*, 16479-16483.
40. Spielberg, E. T.; Edengeiser, E.; Mallick, B.; Havenith, M.; Mudring, A. V. (1-Butyl-4-methyl- pyridinium) Cu($SCN)_2$: A Coordination Polymer and Ionic Liquid. *Chem. Eur. J.* **2014,** *20*, 5338-5345.
41. Harvey, P. D.; Knorr, M. Luminescent Coordination Polymers Built Upon Cu_4X_4 (X = Br,I) Clusters and Mono- and Dithioethers. *Macromol. Rapid Commun.* **2010,** *31*, 808-826.
42. Peng, R.; Li, M.; Li, D. Copper(I) halides: A versatile family in coordination chemistry and crystal engineering. *Coord. Chem. Rev.* **2010,** *254*, 1-18.
43. Wachter, J.; 2013; Vol. 1, p 933.
44. Harvey, P. D.; Knorr, M. Stabilization of $(CuX)_n$ Clusters (X = Cl, Br, I; n=2, 4, 5, 6, 8) in Mono- and Dithioether-Containing Layered Coordination Polymers. *J. Cluster Sci.* **2015,** *26*, 411-459.
45. Harvey, P. D.; Knorr, M. Designs of 3-Dimensional Networks and MOFs Using Mono- and Polymetallic Copper(I) Secondary Building Units and Mono- and Polythioethers: Materials Based on the Cu-S Coordination Bond. *J. Inorg. Organomet. Polym. Mater.* **2016,** *26*, 1174-1197.
46. Liu, Q.; Zhang, W.-H.; Lang, J.-P. Versatile thiomolybdate(thiotungstate)-copper-sulfide clusters and multidimensional polymers linked by cyanides. *Coord. Chem. Rev.* **2017,** *350*, 248-274.
47. Liu, S.-Y.; Zhang, J.-P.; Chen, X.-M. Cu(I) 3,5-Diethyl-1,2,4-Triazolate (MAF-2): From Crystal Engineering to Multifunctional Materials. *Cryst. Growth Des.* **2017,** *17*, 1441-1449.
48. Lapprand, A.; Bonnot, A.; Knorr, M.; Rousselin, Y.; Kubicki, M. M.; Fortin, D.; Harvey, P. D. Formation of an unprecedented $(CuBr)_5$ cluster and a zeolite-type 2D-coordination polymer: a surprising halide effect. *Chem. Commun.* **2013,** *49*, 8848-8850.
49. Juvenal, F.; Langlois, A.; Bonnot, A.; Fortin, D.; Harvey, P. D. Luminescent 1D-and 2D-Coordination Polymers Using CuX Salts (X = Cl, Br, I) and a Metal-Containing Dithioether Ligand. *Inorg. Chem.* **2016,** *55*, 11096-11109.
50. Juvenal, F.; Bonnot, A.; Fortin, D.; Harvey, P. D. The trans-Bis(p-thioetherphenylacetynyl)bis(phosphine)platinum(II) Ligands: A Step towards Predictability and Crystal Design. *ACS Omega* **2017,** *2*, 7433-7443.

51. Bi, M.; Li, G.; Hua, J.; Liu, Y.; Liu, X.; Hu, Y.; Shi, Z.; Feng, S. Two isomers with FSC topology constructed from $Cu_6I_6(DABCO)_4$ and $Cu_8I_8(DABCO)_6$ building blocks. *Cryst. Growth Des.* **2007,** *7*, 2066-2070.
52. Wang, J.; Zheng, S.-L.; Hu, S.; Zhang, Y.-H.; Tong, M.-L. New in situ cleavage of both S-S and S-C(sp_2) bonds and rearrangement reactions toward the construction of copper(I) cluster-based coordination networks. *Inorg. Chem.* **2007,** *46*, 795-800.
53. Hou, Q.; Yu, J.-H.; Xu, J.-N.; Yang, Q.-F.; Xu, J.-Q. A new 3-D two-fold interpenetrated framework with sqp net based on Cu_6I_6 and Cu_8I_8 cluster nodes. *CrystEngComm* **2009,** *11*, 2452-2455.
54. Bai, S.-Q.; Kwang, J. Y.; Koh, L. L.; Young, D. J.; Hor, T. S. A. Functionalized 1,2,3-triazoles as building blocks for photoluminescent POLOs (polymers of oligomers) of copper(I). *Dalton Trans.* **2010,** *39*, 2631-2636.
55. Zhang, Y.; Wu, T.; Liu, R.; Dou, T.; Bu, X.; Feng, P. Three-Dimensional Photoluminescent Frameworks Constructed from Size-Tunable CuI Clusters. *Cryst. Growth Des.* **2010,** *10*, 2047-2049.
56. Zeng, G.; Xing, S.; Wang, X.; Yang, Y.; Ma, D.; Liang, H.; Gao, L.; Hua, J.; Li, G.; Shi, Z.; Feng, S. 3d-4f Metal-Organic Framework with Dual Luminescent Centers That Efficiently Discriminates the Isomer and Homologues of Small Organic Molecules. *Inorg. Chem.* **2016,** *55*, 1089-1095.
57. Zeng, G.; Xing, S.; Wang, X.; Yang, Y.; Xiao, Y.; Li, Z.; Li, G.; Shi, Z.; Feng, S. Synthesis, structures and luminescence properties of 3d-4f heterometallic-organic frameworks (HMOFs) constructed from different copper halide clusters. *CrystEngComm* **2016,** *18*, 4336-4342.
58. Song, Y.; Fan, R.-Q.; Xing, K.; Du, X.; Su, T.; Wang, P.; Yang, Y.-L. Insight into the Controllable Synthesis of Cu(I)/Cu(II) Metal-Organic Complexes: Size-Exclusive Selective Dye Adsorption and Semiconductor Properties. *Cryst. Growth Des.* **2017,** *17*, 2549-2559.
59. Shan, X.-C.; Zhang, H.-B.; Chen, L.; Wu, M.-Y.; Jiang, F.-L.; Hong, M.-C. Multistimuli-Responsive Luminescent Material Reversible Switching Colors via Temperature and Mechanical Force. *Cryst. Growth Des.* **2013,** *13*, 1377-1381.
60. Knorr, M.; Bonnot, A.; Lapprand, A.; Khatyr, A.; Strohmann, C.; Kubicki, M. M.; Rousselin, Y.; Harvey, P. D. Reactivity of CuI and CuBr toward Dialkyl Sulfides RSR: From Discrete Molecular $Cu_4I_4S_4$ and $Cu_8I_8S_6$ Clusters to Luminescent Copper(I) Coordination Polymers. *Inorg. Chem.* **2015,** *54*, 4076-4093.
61. Harvey, P. D.; Bonnot, A.; Lapprand, A.; Strohmann, C.; Knorr, M. Coordination $RC_6H_4S(CH_2)_8SC_6H_4R/(CuI)_n$ Polymers (R (n) = H (4); Me (8)): An Innocent Methyl Group that Makes the Difference. *Macromol. Rapid Commun.* **2015,** *36*, 654-659.
62. Bonnot, A.; Juvenal, F.; Lapprand, A.; Fortin, D.; Knorr, M.; Harvey, P. D. Can a highly flexible copper(I) cluster-containing 1D and 2D coordination polymers exhibit MOF-like properties? *Dalton Trans.* **2016,** *45*, 11413-11421.
63. Takemura, Y.; Nakajima, T.; Tanase, T. Interconversion between ladder-type octanuclear and linear tetranuclear copper(I) complexes supported by tetraphosphine ligands. *Dalton Trans.* **2009**, 10231-10243.
64. Cheng, Y.; Xu, P.; Ding, Y.-B.; Yin, Y.-G. Stoichiometry-dominated in situ formation of iodocuprate clusters and dimethyl-2,2 '-biimidazoles as building units of coordination architectures. *CrystEngComm* **2011,** *13*, 2644-2648.

65. Kursheva, L. I.; Kataeva, O. N.; Gubaidullin, A. T.; Khasyanzyanova, F. S.; Vakhitov, E. V.; Krivolapov, D. B.; Batyeva, E. S. Triisopropyl phosphorotrithioite as a monodantate and a tridentate ligand in complexes with copper(I) halides. *Russ. J. Gen. Chem.* **2003,** *73*, 1516-1521.
66. Goreshnik, E. A.; Ciunik, L. Z.; Gorelenko, Y. K.; Mys'kiv, M. G. Complexation of the 2,4,6-triallyloxy-1,3,5-triazine with copper(I,II) chlorides. Syntheses and crystal structures of $[CuCl_2 . 2C_3N_3(OC_3H_5)_3]$, $[Cu_7Cl_8 . 2 C_3N_3(OC_3H_5)_3]$, and $[Cu_8Cl_8 . 2C_3N_3(OC_3H_5)_3 .2C_2H_5OH$. *Z. Anorg. Allg. Chem.* **2004,** *630*, 2743-2748.
67. Knorr, M.; Khatyr, A.; Aleo, A. D.; El Yaagoubi, A.; Strohmann, C.; Kubicki, M. M.; Rousselin, Y.; Aly, S. M.; Fortin, D.; Lapprand, A.; Harvey, P. D. Copper(I) Halides (X = Br, I) Coordinated to Bis(arylthio)methane Ligands: Aryl Substitution and Halide Effects on the Dimensionality, Cluster Size, and Luminescence Properties of the Coordination Polymers. *Crystal Growth & Design* **2014,** *14*, 5373-5387.
68. Martinez-Alanis, P. R.; Ugalde-Saldivar, V. M.; Castillo, I. Electrochemical and Structural Characterization of Tri- and Dithioether Copper Complexes. *Eur. J. Inorg. Chem.* **2011**, 212-220.
69. Knaust, J. M.; Keller, S. W. Supermolecular coordination isomers: synthesis and crystal structures of four new one-dimensional copper(I) coordination polymers with 1,3-dithiane. *CrystEngComm* **2003,** *5*, 459-465.
70. Frisch, M. J.; Trucks, G. W.; Schlegel, H. B.; Scuseria, G. E.; Robb, M. A.; Cheeseman, J. R.; Montgomery Jr, J. A.; Vreven, T. K. K. N.; LKudin, K. N.; Burant, J. C.; Millam, J. M. *Gaussian 09*. Wallingford, CT, 2004.
71. Hohenberg, P.; Kohn, W. Inhomogeneous electron gas. *Physical Review B* **1964,** *136*, B864-+.
72. Hohenberg, P.; Kohn, W. *J. Phys. Rev.* **1965,** *140*, A1133.
73. Lee, C. T.; Yang, W. T.; Parr, R. G. Development of the Colle-Salvetti correlation-energy formula into a functionnal of the electron-density. *Physical Review B* **1988,** *37*, 785-789.
74. Miehlich, B.; Savin, A.; Stoll, H.; Preuss, H. Results obtained with the correlation-energy density functionals of Becke and lee, Yang and Parr. *Chem. Phys. Lett.* **1989,** *157*, 200-206.
75. Parr, R. G.; Yang, W. *Density-functionnal theory of atoms and molecules*. Oxfor Univ. Press, Oxford U.K., 1989.
76. Salahub, D. R.; Zerner, M. C. *The Challenge of d and f Electrons,* . Amer. Chem. Soc. Washington, D.C.: 1989.
77. Becke, A. D. Density-functional thermochemistry 3. The role of exact exchange. *J. Chem. Phys.* **1993,** *98*, 5648-5652.
78. Bauernschmitt, R.; Ahlrichs, R. Treatment of electronic excitations within the adiabatic approximation of time dependent density functional theory. *Chem. Phys. Lett.* **1996,** *256*, 454-464.
79. Casida, M. E.; Jamorski, C.; Casida, K. C.; Salahub, D. R. Molecular excitation energies to high-lying bound states from time-dependent density-functional response theory: Characterization and correction of the time-dependent local density approximation ionization threshold. *J. Chem. Phys.* **1998,** *108*, 4439-4449.
80. Stratmann, R. E.; Scuseria, G. E.; Frisch, M. J. An efficient implementation of time-dependent density-functional theory for the calculation of excitation energies of large molecules. *J. Chem. Phys.* **1998,** *109*, 8218-8224.
81. Binkley, J. S.; Pople, J. A.; Hehre, W. J. self-consistent molecular orbital methods. 21. Small split-Valence basis-sets for 1st row elements. *J. Am. Chem. Soc.* **1980,** *102*, 939-947.

82. Gordon, M. S.; Binkley, J. S.; Pople, J. A.; Pietro, W. J.; Hehre, W. J. self-consistent molecular-orbital methods .22. small split-valence basis-sets for 2nd-row elements. *J. Am. Chem. Soc.* **1982,** *104*, 2797-2803.
83. Pietro, W. J.; Francl, M. M.; Hehre, W. J.; Defrees, D. J.; Pople, J. A.; Binkley, J. S. self-consistent molecular-orbital methods .24. supplemented small split-valence basis-sets for 2nd-row elements. *J. Am. Chem. Soc.* **1982,** *104*, 5039-5048.
84. Dobbs, K. D.; Hehre, W. J. molecular-orbital theory of the properties of inorganic and organometallic compounds 4 - extended basis-sets for 3rd-row and 4th-row, main-group elements. *J. Comput. Chem.* **1986,** *7*, 359-378.
85. Dobbs, K. D.; Hehre, W. J. molecular-orbital theory of the properties of inorganic and organometallic compounds .5. extended basis-sets for 1st-row transition-metals. *J. Comput. Chem.* **1987,** *8*, 861-879.
86. Dobbs, K. D.; Hehre, W. J. molecular-orbital theory of the properties of inorganic and organometallic compounds .6. extended basis-sets for 2nd-row transition-metals. *J. Comput. Chem.* **1987,** *8*, 880-893.
87. O'Boyle, N. M.; Tenderholt, A. L.; Langner, K. M. cclib: A library for package-independent computational chemistry algorithms. *J. Comput. Chem.* **2008,** *29*, 839-845.
88. Munakata, M.; Wu, L. P.; Kuroda-Sowa, T.; Maekawa, M.; Suenaga, Y.; Nakagawa, S. One-, two- and three-dimensional copper(I) and silver(I) complexes of 2,11-dithia[3.3]paracyclophane. *J. Chem. Soc., Dalton Trans.* **1996**, 1525-30.
89. Maelger, H.; Olbrich, F.; Kopf, J.; Abeln, D.; Weiss, E. Synthesis and crystal structure of Lewis base adducts of copper(I)-halides with dimethyl sulfide and tetrahydrothiophene. *Zeitschrift fuer Naturforschung, B: Chemical Sciences* **1992,** *47*, 1276-80.
90. Lu, W.; Yan, Z.-M.; Dai, J.; Zhang, Y.; Zhu, Q.-Y.; Jia, D.-X.; Guo, W.-J. Coordination Assembly of TTF Derivatives through CuI Bridges. *Eur. J. Inorg. Chem.* **2005**, 2339-2345.
91. Knorr, M.; Guyon, F.; Khatyr, A.; Allain, M.; Aly, S. M.; Lapprand, A.; Fortin, D.; Harvey, P. D. Unexpected Formation of a Doubly Bridged Cyclo-1,2-dithian 1D Coordination Cu_2I_2-Containing Luminescent Polymer. *J. Inorg. Organomet. Polym. Mater.* **2010,** *20*, 534-543.
92. Knorr, M.; Guyon, F.; Khatyr, A.; Strohmann, C.; Allain, M.; Aly, S. M.; Lapprand, A.; Fortin, D.; Harvey, P. D. Construction of $(CuX)_2$ Cluster-Containing (X = Br, I; n=1, 2) Coordination Polymers Assembled by Dithioethers $ArS(CH_2)_mSAr$ (Ar = Ph, p-Tol; m=3, 5): Effect of the Spacer Length, Aryl Group, and Metal-to-Ligand Ratio on the Dimensionality, Cluster Nuclearity, and the Luminescence Properties of the Metal-Organic Frameworks. *Inorg. Chem.* **2012,** *51*, 9917-9934.
93. Peindy, H. N.; Guyon, F.; Khatyr, A.; Knorr, M.; Strohmann, C. Construction of 1D and 2D copper(I) coordination polymers assembled by $PhS(CH_2)_nSPh$ (n = 1, 2) dithioether Ligands: surprising effect of the spacer length on the dimensionality, cluster nuclearity and the fluorescence properties of the metal-organic framework. *Eur. J. Inorg. Chem.* **2007**, 1823-1828.
94. Blake, A. J.; Brooks, N. R.; Champness, N. R.; Crew, M.; Gregory, D. H.; Hubberstey, P.; Schroder, M.; Deveson, A.; Fenske, D.; Hanton, L. R. Topological isomerism in coordination polymers. *Chem. Commun.* **2001**, 1432-1433.
95. Heller, M. A novel huge diamond-like three-fold interpenetrated network of CuI and crown ether. *Z. Anorg, Allg. Chem.* **2006,** *632*, 441-444.
96. Zhang, J.; Xue, Y.-S.; Li, Y.-Z.; Du, H.-B.; You, X.-Z. Cuprous iodide coordination polymers $(CuI)_x(L)_y.z$(solvent) built on linear thioether linkers. *CrystEngComm* **2011,** *13*, 2578-2585.

97. Henline, K. M.; Wang, C.; Pike, R. D.; Ahern, J. C.; Sousa, B.; Patterson, H. H.; Kerr, A. T.; Cahill, C. L. Structure, Dynamics, and Photophysics in the Copper(I) Iodide-Tetrahydrothiophene System. *Crystal Growth & Design* **2014,** *14*, 1449-1458.
98. Bowmaker, G. A.; Knappstein, R. J.; Tham, S. F. Infrared and Raman Spectroscopic study of some groupe 1B halide complexes containing an M_4X_4 core *Aust. J. Chem.* **1978,** *31*, 2137-2143.
99. Turcotte, M.; Harvey, P. D. Characterization of the $\{Ag(dmb)_2^+\}_n$ Oligomers (dmb = 1,8-Diisocyano-*p*-menthane) in Solution. *Inorg. Chem.* **2002,** *41*, 2971-2974.
100. Wyckoff, R. W. G.; Posnjak, E. The crystal structures of the cuprous halides. *J. Am. Chem. Soc.* **1922,** *44*, 30-36.
101. Kim, T. H.; Yang, H.; Park, G.; Lee, K. Y.; Kim, J. gamma-CuI Nanocrystals from Self-Assembled Coordination Polymers. *Chem. Asian J.* **2010,** *5*, 252-255.
102. Zhou, J.; Bian, G.-Q.; Dai, J.; Zhang, Y.; Zhu, Q.-Y.; Lu, W. Luminescent 2-D double-layered polymer, $(CuI)_4(CH_3SCH_3)_3$ ∞, containing helical chains constructed by flower-basket-shaped Cu_4I_4 clusters. *Inorg. Chem.* **2006,** *45*, 8486-8488.
103. Knorr, M.; Pam, A.; Khatyr, A.; Strohmann, C.; Kubicki, M. M.; Rousselin, Y.; Aly, S. M.; Fortin, D.; Harvey, P. D. Reactivity of CuI and CuBr toward Et_2S: a Reinvestigation on the Self-Assembly of Luminescent Copper(I) Coordination Polymers. *Inorg. Chem.* **2010,** *49*, 5834-5844.

SYNOPSIS

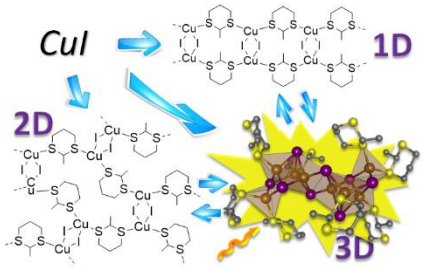

Graphic art

A quasi-predictable design of a luminescent 3D CP containing a Cu_8I_8 cluster, consisting of an unprecedented open dicubane, is made. Furthermore, the interconversion between 1D, 2D and 3D networks has been investigated.